Development of the global chemistry-climate coupled model BCC-GEOS-Chem v2.0: improved atmospheric chemistry performance and new capability of chemistry-climate interactions

Ruize Sun[1#], Xiao Lu[2#], Haipeng Lin[3], Tongwen Wu[4,5], Xingpei Ye[1], Lu Shen[1], Xuan Wang[6], Haolin Wang[2], Jingyu Li[2], Ni Lu[1], Jiayin Su[2], Jie Zhang[4,5], Fang Zhang[4,5], Xiaoge Xin[4,5], Xiong Liu[7], Xiao Yang[2], Lin Zhang[1,8,9,*]

[1]Department of Atmospheric and Oceanic Sciences, School of Physics, Peking University, Beijing, China
[2]School of Atmospheric Sciences, Sun Yat-sen University, Zhuhai, Guangdong, China
[3]John A. Paulson School of Engineering and Applied Sciences, Harvard University, Cambridge, MA, United States of America
[4]State Key Laboratory of Disaster Weather Science and Technology, CMA EMPC
[5]CMA Earth System Modeling and Prediction Centre, China Meteorological Administration, Beijing, China
[6]School of Energy and Environment, City University of Hong Kong, Hong Kong SAR, China
[7]Center for Astrophysics | Harvard & Smithsonian, Cambridge, MA 02138, USA
[8] Institute of Carbon Neutrality, Peking University, Beijing, China
[9] Center for Environment and Health, Peking University, Beijing, China

 # These authors contributed equally to this work.

Correspondence to: Lin Zhang (zhanglg@pku.edu.cn)

Abstract. Interactions between atmospheric chemical compounds and climate have a great impact on the earth system and atmospheric chemistry. However, the online two-way chemistry-climate coupled model, an indispensable tool for quantifying chemistry-climate interactions and projecting future air quality with climate change, remains sparse due to the considerable challenge in model complexity and computational resources. We present the development and evaluation of BCC-GEOS-Chem v2.0, which couples the GEOS-Chem chemical transport model (v14.0.1) with the Beijing Climate Centre Earth System Model (BCC-ESM). Based on the modular framework of BCC-GEOS-Chem v1.0, BCC-GEOS-Chem v2.0 further couples the Harmonized Emissions Component (HEMCO) to manage anthropogenic emission inventories and natural emissions, updates the chemical mechanism, includes the feedback of aerosols and greenhouse gases, and develops the capability for high-resolution simulation. The standard chemical mechanism in the BCC-GEOS-Chem v2.0 features a comprehensive O_x-NO_x-VOC-halogen-aerosol chemical scheme for the troposphere and the stratosphere. We further evaluate the performance of the BCC-GEOS-Chem v2.0 simulation in representing atmospheric chemistry and compare with the model outputs from the BCC-GEOS-Chem v1.0 and BCC-AGCM-Chem over the simulated time period (2012–2014) at a spatial resolution of T42L26 (approximately 2.8°× 2.8° and 26 vertical layers with a top at 2.914 hPa). BCC-GEOS-Chem v2.0 accurately depicts the primary seasonal and spatial distributions of tropospheric ozone observed by multiple instruments, showing small global mean biases of -2.1−1.8 ppbv for mid-tropospheric (700-400 hPa) ozone concentrations relative to satellite observations, along with a high spatial correlation coefficient (r) of 0.77−0.92 for individual seasons. It also demonstrates improved performance in simulating tropospheric carbon monoxide (CO), nitrogen dioxide (NO_2), formaldehyde (CH_2O) and surface $PM_{2.5}$ compared to both BCC-GEOS-Chem v1.0 and the BCC-AGCM-Chem. The diagnostics of tropospheric ozone budgets (a global tropospheric ozone burden of 355 Tg) and OH concentrations (0.97×10^6 molecule cm^{-3}) are generally consistent with observation-constrained estimates and multi-model assessment. With the inclusions of aerosol-radiation and aerosol-cloud interactions, BCC-GEOS-Chem v2.0 reproduces the expected impacts of aerosols on radiative and cloud properties, e.g., decreasing shortwave downward solar radiation and outgoing longwave radiation, increasing cloud liquid water, and suppressing precipitation. The high-resolution simulation at T159L72 (approximately 0.75° × 0.75° and 72 vertical layers with a top at 0.01 hPa) further improves the model capability in resolving the fine-scale plume transport dynamics and the pollution hotspot of NO_2 and $PM_{2.5}$, as well as the low ozone concentration in high-NO_x environment in wintertime China. The development of the BCC-GEOS-Chem v2.0 model provides a powerful tool to study climate-chemistry interactions and for future projection of global atmospheric chemistry and regional air quality.

1 Introduction

Interactions between atmospheric chemical compounds and climate have a profound impact on the earth system and atmospheric chemistry (Isaksen et al., 2009; Fiore et al., 2012). Climate modulates the emissions of chemical compounds from natural and anthropogenic sources, as well as the chemical kinetics, deposition process, and the transport of the advected species (Jacob and Winner, 2009; Abel et al., 2017; Lu et al., 2019a). In turn, changes in greenhouse gases and aerosols alter the radiative budgets of the climate system (Haywood and Boucher, 2000; Lohmann and Feichter, 2005; Fan et al., 2016; Alizadeh-Choobari and Gharaylou, 2017). There is an increasing number of climate system models that incorporate interactive atmospheric chemistry from the Phase 5 to the Phase 6 of the Coupled Model Intercomparison Project (CMIP5&CMIP6) (IPCC AR5, 2013, IPCC AR6, 2021). These models play a pivotal role in supporting the Intergovernmental Panel on Climate Change (IPCC) assessment reports, especially in assessing the contribution of both long-lived and short-lived climate forcers (SLCFs) to global change. However, many existing CMIP models employ highly simplified representations of atmospheric chemistry (IPCC AR5, 2013, Working Group I, Chapter 9, Appendix Table 9. A.1), For example, only 10 of the 39 models participated in CMIP5 simulated atmospheric chemistry interactively, which introduces substantial uncertainties in quantitative assessments, particularly for SLCFs with high spatiotemporal heterogeneities. Advancing the mechanistic fidelity of atmospheric chemistry in Earth system models is therefore critical for reducing these uncertainties. We previously developed the global atmospheric chemistry general circulation model BCC-GEOS-Chem v1.0 (Lu et al., 2020), a one-way online coupling of Beijing Climate Centre atmospheric general circulation model (BCC-AGCM) and the GEOS-Chem chemical transport model. Here, we present the development of a global chemistry-climate coupled model BCC-GEOS-Chem v2.0, with improved representation of comprehensive troposphere-stratosphere chemistry and new capability to account for radiative-cloud feedbacks from SLCFs, and evaluate its performance in reproducing present-day atmospheric composition and feedbacks to climate system.

BCC-GEOS-Chem is designed to integrate GEOS-Chem within BCC-ESM, the Beijing Climate Centre Earth system model developed by the China Meteorological Administration (CMA). BCC-ESM is a fully coupled Earth system model with interactive atmosphere, land, ocean, and sea-ice components. The first BCC-ESM version (BCC-ESM1) utilizes the BCC-AGCM-Chem as the atmospheric chemistry general circulation model, with the chemistry scheme originating from the MOZART2 (Model for OZone And Related chemical Tracers, version 2), a troposphere-only chemical model developed by the National Center for Atmospheric Research (Horowitz et al., 2003). BCC-ESM1 has participated in a number of research initiatives endorsed by CMIP6, including the Aerosol Chemistry Model Intercomparison Project (AerChemMIP; Collins et al., 2017) and the Coupled Climate–Carbon Cycle Model Intercomparison Project (C4MIP; Jones et al., 2016). GEOS-Chem, initially described by Bey et al. (2001), is a global three-dimensional chemical transport model that includes a detailed ozone–NO_x–VOC–aerosol–halogen chemistry scheme. It can both be used offline as a chemical transport model driven by archived meteorological fields or as an online chemical module driven by weather and climate models (Long et al., 2015; Hu et al., 2018; Lin et al., 2020; Fritz et al., 2022). A defining feature of the GEOS-Chem model lies in its continuous integration of scientific advancements through frequent community-driven updates on model mechanisms and structure (https://github.com/geoschem/geos-chem). The model undergoes rigorous validation through comprehensive benchmarking protocols and continuous evaluation against observational datasets contributed by the international research community (e.g., Hu et al., 2017; Wang et al., 2022). Its cloud-based architecture ensures open accessibility and computational reproducibility. These characteristics establish GEOS-Chem as a state-of-the-art atmospheric chemistry module in Earth System Models, providing robust scientific capabilities and operational reliability for wide applications on air quality and climate.

BCC-GEOS-Chem v1.0 resulted from the integration of the GEOS-Chem chemical module version 11-02b into the atmospheric component of BCC-ESM, *i.e.,* the BCC-AGCM (Lu et al., 2020). This is done by separating the chemical module (which simulates all local processes, including convection, chemistry, deposition, and emissions) from the simulation of advective transport in GEOS-Chem, allowing the GEOS-Chem chemical module to operate on one-dimensional vertical columns in a grid-independent manner (Long et al., 2015; Eastham et al., 2018). Transport is done separately in the BCC-AGCM as part of the simulation of atmospheric dynamics. Consequently, the GEOS-Chem chemical module can be coupled with any ESM grid, where the ESM manages dynamics (transport), allowing adjustable grid types and resolutions. When utilized as an online chemical module in ESMs, GEOS-Chem shares the same code as the offline GEOS-Chem for local processes (convection, chemistry, deposition, and emissions) while using online meteorological fields from the ESMs (Long et al., 2015). This capability ensures that scientific advancements in GEOS-Chem, contributed by the global research community, can be easily incorporated into ESMs, allowing the chemistry of ESM to stay aligned with the latest version of GEOS-Chem. Validation against suborbital and satellite datasets demonstrates that the BCC-GEOS-Chem v1.0 model successfully reproduces observed spatiotemporal patterns of SLCFs, while also delivering an improved representation of tropospheric oxidation processes. Key metrics such as tropospheric ozone chemical production/loss and the global hydroxyl radical (OH) budget in BCC-GEOS-Chem v1.0 show enhanced consistency with observational constraints or multi-model assessments, compared with the BCC-AGCM-Chem model implemented in BCC-ESM1 (Lu et al., 2020).

However, there are several limitations in BCC-GEOS-Chem v1.0. Firstly, the GEOS-Chem v11-02b integrated in the BCC-GEOS-Chem v1.0 model employs the TropChem chemical mechanism, which comprises 74 advected tracer species and 91 non-advected species. While this configuration represented a state-of-the-art understanding of atmospheric chemical processes at its development stage, subsequent updates of the chemical mechanism and deposition scheme have been introduced to GEOS-Chem. For example, a more comprehensive halogen chemistry (Wang et al., 2021) and aromatic oxidation mechanism (Bates et al., 2024) have been implemented, demonstrating improved agreement with in situ measurements. The number of chemical species in GEOS-Chem has now expanded to over 200. In particular, the TropChem mechanisms in BCC-GEOS-Chem v1.0 do not include interactive stratospheric chemistry, despite the critical role of stratospheric chemistry in modulating global atmospheric dynamics. Secondly, BCC-GEOS-Chem v1.0 only includes direct radiative feedback of long-lived greenhouse gases such as carbon dioxide, while radiative-cloud feedbacks associated with chemically active SLCFs such as aerosols are not considered. This key limitation restricts its capability to explore climate-chemistry interactions. Furthermore, BCC-GEOS-Chem v1.0 employs hard-coded emission inputs, requiring manual source code modifications and software recompilation to update emission inventories–a computationally inefficient workflow for iterative experimentation and not adapt to the continuously updated chemical species with rapid updates to the GEOS-Chem chemical mechanism. These limitations have motivated the development of BCC-GEOS-Chem v2.0, which aims to address these limitations through three key advancements: (1) implementation of state-of-the-art interactive troposphere-stratosphere chemical mechanisms aligned with the latest GEOS-Chem updates, (2) establishment of two-way coupling between atmospheric chemistry and climate to enable interactive feedback processes, and (3) architectural optimization of the codebase to enhance flexibility for file inputs/outputs (including emission inventory) and for future model development.

This paper presents an overview of the BCC-GEOS-Chem v2.0 model and evaluates the model simulation of present-day atmospheric chemistry and climate with the new capability of aerosol feedbacks. In Section 2, we describe the model framework, individual components, and key updates from BCC-GEOS-Chem v1.0. In Section 3, we introduce the observational dataset for model evaluation and the design of model simulation experiment, including a 3-year (2012-2014) base simulation of BCC-GEOS-Chem v2.0 for comparison with results from the BCC-AGCM-Chem (the chemical module for BCC-ESM1) and BCC-GEOS-Chem v1.0 at the same spatial and temporal resolution, as well as sensitivity simulations for assessing aerosols feedback on the radiation and cloud properties. In Section 4, we evaluate the simulated gaseous pollutants and aerosols with satellite and suborbital observations, and also diagnose the global tropospheric ozone burden and budget. In Section 5, we assess the influences of Aerosol-Radiation-Interactions (ARIs) and Aerosol-Cloud-Interactions

(ACIs) on radiative fluxes and cloud properties. In Section 6, we briefly introduce the capability of BCC-GEOS-Chem v2.0 to perform at high resolution. Future plans for model development and summary are presented in Section 7.

2 Development and description of the BCC-GEOS-Chem v2.0

Figure 1 presents an architectural overview of the BCC-GEOS-Chem v2.0. The previous version BCC-GEOS-Chem v1.0 only enables interactive atmosphere and land modules, with other components such as ocean and sea ice defined as boundary conditions. The BCC-GEOS-Chem v2.0 has now evolved into a fully coupled Earth system model that integrates interactively the atmospheric dynamic model of BCC-AGCM, the land surface model of BCC Atmosphere and Vegetation Interaction Model (BCC-AVIM), the oceanic component of Modular Ocean Model (MOM), and the sea ice model of SIS (Section 2.1). These components interact through bidirectional flux exchanges of momentum, energy, water, and carbon facilitated by coupler. The BCC-GC-HEMCO interface (Section 2.2), embedded in BCC-AGCM, is the key component linking the atmospheric module, the Harmonized Emissions Component (HEMCO) for processing emission inventories and necessary geography data (Keller et al., 2014; Lin et al., 2021; Section 2.3.1), and the GEOS-Chem chemical module (Section 2.3.2 and 2.3.3). Functional advancements that enable feedbacks from aerosol and greenhouse gases to dynamics are introduced separately in Section 2.4.

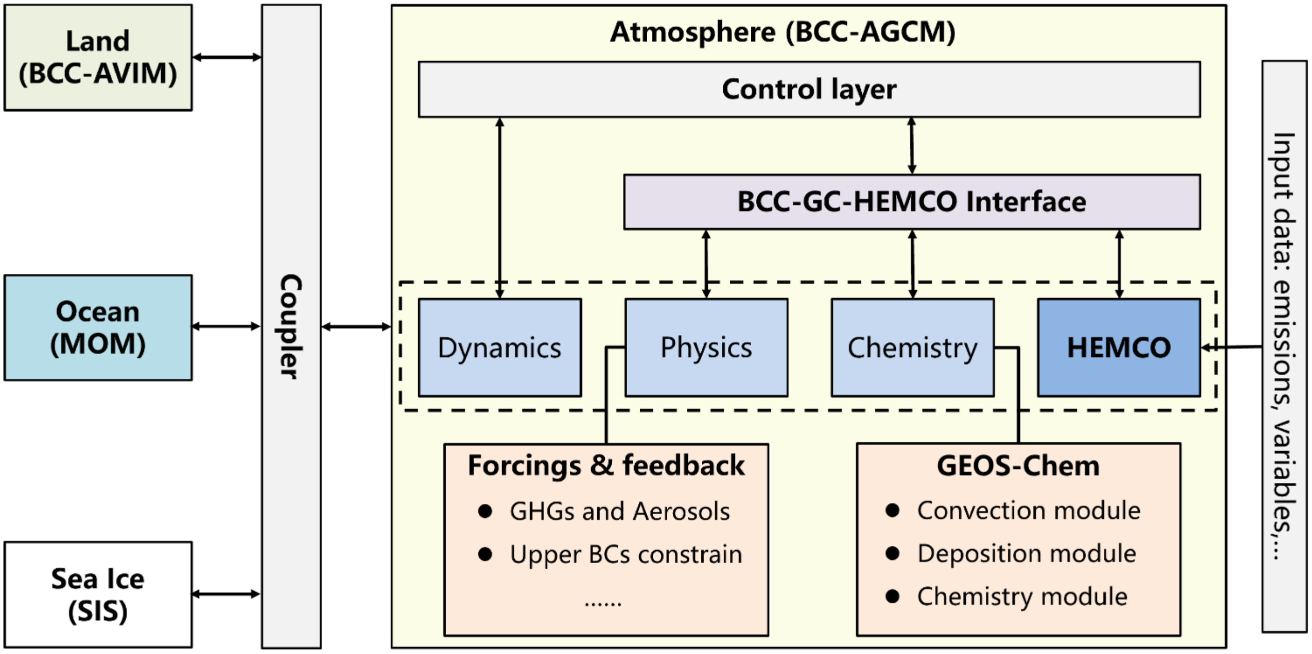

Figure 1. Architectural overview of the BCC-GEOS-Chem v2.0.

2.1 Atmospheric, Land, Oceanic, and Sea ice components of BCC-GEOS-Chem v2.0

The atmospheric component BCC-AGCM is a global atmospheric spectral model, which can be configured at multiple horizontal and vertical resolution (e.g., T42L26, T159L72, T382L72, where "T" and affiliated number represent the number of maximum wavenumbers set by triangular truncation, "L" and affiliated number represent number of vertical levels). In this study, we use BCC-AGCM version 4.0 at two spectral resolutions, *i.e.*, T42L26 (approximately 2.8° latitude × 2.8° longitude horizontally and 26 fixed vertical hybrid layers extending from the surface to 2.914 hPa), and T159L72 (approximately 0.75° latitude × 0.75° longitude horizontally and 72 fixed vertical hybrid layers extending from the surface to 0.01 hPa). The vertical discretization in BCC-ESM follows a hybrid sigma-pressure system: upper layers use pressure coordinates, while lower levels transition to sigma coordinates that are purely terrain-following at the surface. We primarily discuss the results of the T42L26 resolution while also comparing them with those from T159L72 in Section 6. The advection of all tracers in BCC-AGCM is handled using a semi-Lagrangian scheme (Williamson and Rasch, 1989), while vertical diffusion within the boundary layer is parameterized based on the approach of Holtslag and Boville (1993). Details of physical processes and the dynamical framework of BCC-AGCM are described in Wu et al. (2019).

BCC-AVIM is an advanced land model with a terrestrial carbon cycle, which includes the biophysical module, plant physiological module, and soil carbon–nitrogen dynamic module. The biophysical module simulates the exchange of energy, water, and carbon among the atmosphere, plant canopy, and soil, incorporating 10 soil layers and up to 5 snow layers. The physiological module performs key vegetation processes, including photosynthesis, respiration, turnover, and mortality, and diagnoses resulting changes in biomass. The soil carbon-nitrogen dynamic module models biochemical processes, such as the conversion and decomposition of soil organic carbon. In this study, we use BCC-AVIM version 2.2. The detailed description of BCC-AVIM2 can be found in Li et al. (2019).

The oceanic component MOM employs a tripolar grid with a horizontal resolution of 1° longitude by 1/3° latitude between 30°S and 30°N, while transitioning to 1° longitude by 1° latitude poleward of 60°S and 60°N (Wu et al. 2020). There are 40 z levels in the vertical, with 13 levels placed between the surface and a depth of 300 m in the upper ocean. Carbon exchange between the atmosphere and ocean is computed online in MOM using a biogeochemistry module based on the protocols established by the Ocean Carbon Cycle Model Intercomparison Project – Phase 2 (OCMIP2). In this study, we use MOM version 5. The sea ice component SIS has the same horizontal resolution as MOM. It has three vertical layers, including one layer of snow cover and two layers of equally sized sea ice. Additional information about the MOM oceanic component and SIS sea ice component is available in Wu et al. (2013, 2019).

Interaction among the components is achieved through bidirectional flux exchanges of momentum, energy, water, and carbon using the coupler adapted from National Centre for Atmospheric Research (NCAR) flux coupler (Craig et al., 2012;

Wu et al., 2019). The coupling under different resolution is achieved using area-weighted or bilinear interpolation schemes that preserve the global integrals of energy, momentum, and mass.

2.2 BCC-GC-HEMCO Interface

The BCC-GC-HEMCO interface (Section 2.2) serves as a central coupler between the atmospheric module, an independent emission handling module (HEMCO, version 3.6.2, DOI: 10.5281/zenodo.7692950), and the GEOS-Chem chemical module (version 14.0.1, DOI: 10.5281/zenodo.7271960), as illustrated in Figure 1. It handles the transfer of meteorological variables, emissions, and necessary geography data, and the concentrations of atmospheric constituents between these components. A key difference in the interface design compared with BCC-GEOS-Chem v1.0 is the implementation of HEMCO as a standalone emission processing module. At each chemical time step, meteorological variables (Table S2) and atmospheric constituent concentrations are passed from BCC-AGCM to GEOS-Chem and HEMCO through the BCC-GC-HEMCO interface. HEMCO returns emission fluxes, diagnosed from read-in offline anthropogenic emission inventory and online algorithms for specific natural sources using inputted meteorological fields (Section 2.3.1), to BCC-AGCM. The GEOS-Chem chemistry module is invoked to sequentially perform convection, dry deposition, gas and aerosol chemistry, and wet deposition. Updated chemical information (e.g., concentration of advected species) is then passed back to BCC-AGCM through the interface. BCC-AGCM then updates the concentrations of chemical species with input fluxes (emission fluxes from HEMCO and deposition fluxes diagnosed in GEOS-Chem) through turbulent mixing, and continues to perform advective transport of the chemical species as part of the simulation of atmospheric dynamics. Minor modifications to the GEOS-Chem source code were made to accommodate the BCC-GC-HEMCO interface, which have been merged to the GEOS-Chem main code branch (https://github.com/geoschem/geos-chem, last access: 1 April 2025) to ensure future compatibility between BCC and GEOS-Chem. With the establishment of the BCC-GC-HEMCO interface, in theory, future updates of GEOS-Chem and HEMCO in the BCC-GEOS-Chem model would only require downloading and substituting the corresponding source code, avoiding significant modifications to the source code.

2.3 Key processes in BCC-GEOS-Chem v2.0

Here we introduce how emission, chemistry, and dry and wet deposition of atmospheric constituents are processed in BCC-GEOS-Chem v2.0.

2.3.1 Emissions

The Harmonized Emissions Component (HEMCO) was initially developed by Keller et al. (2014) for integrating emission inventories and algorithms in the GEOS-Chem model. It can provide emissions from a database library of emission inventories with the capability to select, add, mask, and scale emissions as configured by a text-based configuration file, as well as a collection of built-in algorithms, referred to as “extensions”, which calculate climate-sensitive emissions such as biogenic, lightning, dust, oceanic sources based on environmental data and model state. The version 3.0 developed by Lin et al. (2021) further modularized HEMCO to enable coupling to the Community Earth System Model (CESM), while maintaining a shared core for computing emissions for any other ESM. The enhanced modularity and flexibility of HEMCO facilitates its seamless integration with the BCC-GEOS-Chem. This architecture also enables efficient incorporation of community-driven updates to emission inventories or algorithms, without the need for modification and compilation of model source code in other parts of BCC-GEOS-Chem model. The implementation of HEMCO as a standalone emission processing module in BCC-GEOS-Chem v2.0 demonstrates a substantial improvement over BCC-GEOS-Chem v1.0. In BCC-GEOS-Chem v1.0, all emission inventories were directly hard-coded without a unified management framework, making it difficult to adapt to the continuously updated chemical species in the context of rapid updates in the GEOS-Chem chemical mechanism (Lu et al, 2020).

We use HEMCO in BCC-GEOS-Chem v2.0 to manage offline anthropogenic emissions, as well as natural emissions including biogenic VOCs (Guenther et al., 2012), soil NO_x (Hudman et al., 2012), dust (Zender et al., 2003) and sea salt (Gong, 2003). These natural emissions can be either calculated online using algorithms that are already implemented in HEMCO and driven by meteorological fields provided by BCC-AGCM, or read from pre-archived files using the same algorithms driven by other meteorological fields (e.g. Weng et al., 2020). Anthropogenic inventories are obtained from the Community Emissions Data System (CEDS) emission inventory version 2 (McDuffie et al. 2020). Monthly mean biomass burning emissions are from the Global Emissions Database version 4 (GFED4; Randerson et al., 2018). Calculation of lightning emissions of NOx is performed in BCC-AGCM rather than in HEMCO for convenience because of its strong link to cloud-top height (Price and Rind, 1992). Figure S1 shows the spatial distributions of key anthropogenic and natural emissions averaged over 2012-2014. Table S1 compares the emissions in BCC-GEOS-Chem v2.0 with those for BCC-GEOS-Chem v1.0 and BCC-AGCM-Chem. Overall, the emission magnitudes and spatial patterns in BCC-GEOS-Chem v2.0 demonstrate comparable characteristics to both BCC-GEOS-Chem v1.0 and BCC-AGCM-Chem, while also remaining consistent with values reported in the literature across different models.

2.3.2 Atmospheric chemistry

BCC-GEOS-Chem v2.0 uses GEOS-Chem v14.0.1 (https://zenodo.org/records/7271974, The International GEOS-Chem Community, 2022) as its chemical module. The standard chemical mechanism in GEOS-Chem v14.0.1 features a comprehensive O_x-NO_x-VOC-halogen-aerosol chemistry in unified tropospheric–stratospheric chemistry extension (UCX) scheme (Eastham et al., 2014). The scheme includes 220 advected chemical species and 914 gas-phase chemical reactions through the Kinetic PreProcessor (KPP) (Damian et al., 2002; Lin et al., 2023). The number of advected tracers is much higher than that in GEOS-Chem v11-02b used in BCC-GEOS-Chem v1.0, where only 74 chemical species were advected in troposphere-only chemistry. Updates on chemistry mechanism from GEOS-Chem v11-02b to GEOS-Chem v14.0.1 are archived at https://github.com/geoschem/geos-chem/releases.

The capability to simulate interactive stratospheric chemistry in BCC-GEOS-Chem v2.0 represents a major improvement compared to BCC-GEOS-Chem v1.0 and BCC-AGCM-Chem. BCC-AGCM-Chem does not include stratospheric chemistry, all chemical species in the stratosphere are relaxed to monthly climatological values from CMIP6 data package (Wu et al., 2020). BCC-GEOS-Chem v1.0 incorporates troposphere-only chemical schemes from GEOS-Chem v11-02b. However, it still lacks interactive stratospheric chemistry despite including a simple linearized ozone parameterization (LINOZ) (McLinden et al., 2000) (Lu et al., 2020). Interactive stratospheric chemistry is now available in BCC-GEOS-Chem v2.0 through the UCX scheme. The scheme describes gas-phase kinetic chemistry with explicit modelling of atomic oxygen and halogens, photochemistry using the Fast-JX scheme, heterogeneous chemistry, and the chemical formation and thermodynamic of stratospheric aerosols (Eastham et al., 2014). Implementation of the UCX scheme within the GEOS-Chem "Classic" framework (driven by reanalysis meteorological fields) has demonstrated the capability to accurately reproduce stratospheric ozone distributions and Antarctic ozone depletion, while also capturing the stratospheric lifetimes of source gases (Eastham et al., 2014).

BCC-GEOS-Chem v2.0 describes the chemical formation and thermodynamics of multiple aerosol components, including primary dust, sea salt, primary organic carbon aerosol (POC), primary black carbon aerosol (BC), secondary inorganic aerosols (sulfate, nitrate, ammonium), and secondary organic aerosols (SOAs). Sea salt aerosol masses are simulated in two size ranges: the accumulation mode (dry radii between 0.1 and 0.5 μm) and the coarse mode (dry radii between 0.5 and 4 μm) (Jaeglé et al., 2011). Dust aerosol masses are simulated in four size ranges (radii of 0.1-1.0, 1.0-1.8, 1.8-3.0, and 3.0-6.0 μm; Fairlie et al., 2007). Details of aerosol chemistry and its interaction with gas-phase chemistry are provided in Lu et al. (2020). Compared to BCC-GEOS-Chem v1.0, key updates of aerosol chemistry include the improved heterogeneous chemistry (e.g. updates in N_2O_5, NO_3, NO_2 reactive uptake, sub-grid cloud NO_y chemistry, aerosol nitrate photolysis) and the ISORROPIA Ⅱ (Fountoukis and Nenes, 2007) thermodynamic module. The aerosols feedback on radiation and cloud is implemented in BCC-GEOS-Chem v2.0, as will be introduced in Section 2.4.

2.3.3 Dry and Wet Deposition

Dry deposition of gas and aerosols in BCC-GEOS-Chem v2.0 are conducted using the GEOS-Chem standard code, following BCC-GEOS-Chem v1.0. The model estimates deposition velocity following the resistance-in-series scheme (Wesely, 1989), and also includes gravitational settling of particles as described in Zhang et al. (2001). The scheme requires the input of geography data such as land types and leaf area index (LAI) to yield surface roughness and canopy resistance. Here we provide two options in BCC-GEOS-Chem v2.0. Firstly, we can obtain archived land types (Olson et al., 2001) and the LAI data for each land type from Moderate Resolution Imaging Spectroradiometer (MODIS) used in GEOS-Chem v14.0.1. Alternatively, we can obtain the land types and LAI information from the BCC-AVIM through the coupler, and then computes dry deposition through the GEOS-Chem routines, as done in BCC-GEOS-Chem v1.0. The latter option requires reconciliation of land types (73 categories) used in GEOS-Chem with those used in BCC-AVIM (22 categories) (Lu et al., 2020). The key advantage of the latter option is that the land surface parameters used for dry deposition align with those generated by the land surface model, thereby improving its utility for studying atmosphere-land surface interactions. However, uncertainties inherent to the land surface model simulations may propagate into atmospheric chemistry calculations. Both options can be applied in BCC-GEOS-Chem v2.0. In this study, we employ the first option as it offers more detailed vegetation classifications (73 vs 22 categories), ensuring improved compatibility and representation within the GEOS-Chem dry deposition parameterization.

Wet deposition of aerosols and soluble gases by precipitation is calculated by the wet deposition module in GEOS-Chem, following BCC-GEOS-Chem v1.0, which accounts for scavenging in convective updrafts, in-cloud rainout, and below-cloud washout (Liu et al., 2001). In particular, the convective transport of chemical tracers and scavenging in the updrafts is performed using the GEOS-Chem convection scheme, driven by convection variables diagnosed from BCC-AGCM, instead of using the convection module in BCC-AGCM-Chem described by Wu et al. (2020). This is because the BCC-AGCM-Chem scheme for wet deposition is hard-coded, incompatible with the updated chemical species, and lacks the scavenging of water-soluble species in convective updrafts, which may cause high bias in aerosol concentrations in the upper troposphere (Lin et al., 2024).

2.4 The feedback of aerosols and greenhouse gases

One significant update in BCC-GEOS-Chem v2.0, relative to BCC-GEOS-Chem v1.0, is the incorporation of the direct (radiation) and indirect (cloud) climate effects of greenhouse gases and aerosols. This incorporation relies on the radiative transfer module already implemented in BCC-ESM1 (Wu et al., 2020). The longwave radiative transfer scheme is based on an absorptivity/emissivity formulation detailed by Ramanathan and Downey (1986), and incorporates explicit parameterization for the major absorbers (Collins et al., 2002a; Kiehl and Briegleb, 1991; Ramanathan and Dickinson, 1979). The shortwave radiation scheme parameterizes gaseous absorption over 19 discrete spectral and pseudo-spectral intervals, as well as the scattering and absorption by cloud droplets and aerosols (Briegleb et al., 1992; Collins et al., 1998). Among the gaseous absorbers, BCC-GEOS-Chem v2.0 prescribes surface mixing ratios of long-lived greenhouse gases (e.g. N_2O, CFC11, and CFC12) and methane using CMIP6 historical forcing data (Section 3), but allows the chemistry and transport of these gases. The use of prescribed surface methane concentrations instead of methane emissions is to ensure a realistic methane distribution in the model, as there are substantial uncertainties associated with its poorly constrained global source–sink balance (Lu et al., 2021; Saunois et al., 2025). However, such configuration limits the representation of full methane-OH feedback in the model. H_2O and ozone are not constrained and are fully diagnosed in BCC-GEOS-Chem v2.0.

The aerosol direct effect is calculated based on the mass mixing ratios of bulk aerosols, which are prognostic variables in the GEOS-Chem chemical module. Derivation of aerosol single-scattering properties follow a lookup table approach following Community Atmosphere Model (CAM; Collins et al., 2004). Based on the Optical Properties of Aerosols and Clouds (OPAC) dataset, optical properties of sea salt, OC, and BC are hypothesized to be identical to those of soot and water-soluble aerosols (Hess et al., 1998). Following Wang et al. (2008b), sulfate and nitrate particles are assumed to share the optical properties of ammonium sulfate, while dust optical properties are calculated using Mie theory for each size bin (Zender et al., 2003). Aerosols across different size bins are assumed to be externally mixed in the calculation of bulk aerosol single-scattering properties. The derived radiative properties are subsequently used in radiative transfer calculation.

The indirect effects of aerosols involve their role as cloud condensation nuclei and their influence on cloud properties and precipitation (Rosenfeld et al., 2008). The diagnostic cloud droplet number concentration N_d is calculated using the empirical function Eq. (1) suggested by Quaas et al. (2006):

$$N_d = \exp\left(a_0 + a_1 \ln m_{aer}\right) , \tag{1}$$

where m_{aer} is the total mass fraction of all hydrophilic aerosols diagnosed from the GEOS-Chem chemical module. a_0 and a_1 are parameters ($a_0 = 5.1$ and a_1=0.41) (Boucher and Lohmann, 1995).

The cloud droplet effective radius R_e is estimated by Eq. (2) according to Peng and Lohmann (2003):

$$R_e = \beta R_v = \beta \sqrt[3]{\frac{3LWC}{4\pi\rho_w N_d}} , \tag{2}$$

where β is a scaling factor. ρ_w is the water density, and LWC is the cloud liquid water content. Both ρ_w and LWC are diagnosed by BCC-AGCM.

The aerosol-activated cloud droplets then exert impacts on cloud properties and precipitation, which is taken into account in the parameterization of cloud microphysics processes. The detailed treatment of the aerosols feedback on precipitation can be found in Wu et al (2020). The current approach for describing the aerosol feedback uses a bulk-mass representation of aerosols in BCC-GEOS-Chem v2.0. This approach is similar to that used in the majority of CMIP5 models, since only two of these models include online size-resolved aerosol microphysics (Kodros and Pierce, 2017). This bulk-mass representation of aerosols is computationally efficient, but does not consider how aerosol microphysics (nucleation, condensation, and coagulation) shape the size distribution. For future model development, we hope to explicitly describe aerosol size distributions by integrating size-resolved schemes such as the Advanced Particle Microphysics (APM) scheme (Yu and Luo, 2009) and the TwO-Moment Aerosol Sectional (TOMAS) microphysics packages (Kodros and Pierce, 2017). These two schemes are available in GEOS-Chem and simulate more accurately the size dependency of aerosol chemistry and microphysics, but are not yet integrated in BCC-GEOS-Chem v2.0 because these two schemes are currently incompatible with the GEOS-Chem column structure.

3 Model simulation setup and observations for model evaluation

3.1 Setup of model experiments

We perform BCC-GEOS-Chem v2.0 simulations and compare the modelled concentrations of key SLCFs against observations and outputs from BCC-GEOS-Chem v1.0 (Lu et al., 2020) and BCC-AGCM-Chem (used in BCC-ESM1, Wu et al.,2020). These three models represent three generations of development in the atmospheric chemistry module of the BCC Earth System Model. The simulations are performed from 2011 to 2014, with the first year as model spin-up following previous studies (Lu et al. 2020; Schwantes et al., 2022; Fritz et al., 2022). We selected this simulation period because the output of BCC-GEOS-Chem v1.0 and BCC-AGCM-Chem are available for the same time frame and resolution from Lu et al. (2020) and Wu et al. (2020), respectively. These three models are configured with free-running meteorology and currently do not support nudging or constraining of meteorological fields to reanalysis.

The initial conditions for atmospheric dynamics and physics in 2011 are obtained from the historical simulations (1850-2014) conducted by BCC-ESM1 under the CMIP6 framework, and initial states of chemical tracers are obtained from a GEOS-Chem simulation over 1995-2017 (Wang et al., 2022). The model results in 2012-2014 are used for evaluation and comparison. External forcing data, including historical concentrations of long-lived greenhouse gases (CO_2, N_2O, CFCs) and methane, land use forcing, and solar forcing are obtained from the Earth System Grid Federation (ESGF). We note that since BCC-AGCM-Chem has no interactive stratospheric chemistry, stratospheric species (O_3, CH_4, N_2O, NO, NO_2, HNO_3, CO, and N_2O_5) concentrations at the top two layers are set to prescribed monthly climatological values from CMIP6 data package as upper boundary conditions, and their concentrations from below the top two layers to the tropopause are relaxed with a relaxation time of 10 d towards the climatological values (Wu et al., 2020). BCC-GEOS-Chem v2.0 eliminates the need for the relaxation of stratospheric chemical species to prescribed fields, since these species can now be calculated interactively using the UCX chemical scheme. However, upper boundary conditions for O_3 and NO_x are still applied to the top two model layers. We also note that the differences of chemical constituents from the three models are not solely due to the chemical mechanisms, but may also arise from variations in the emission inventory, treatment of physical and dynamical processes, inclusion of radiative and cloud feedback, and other factors (e.g., interactions with the ocean model) (Table 1 and Table S1).

Table 1. Summary of the model features and configuration for BCC-GEOS-Chem v2.0, BCC-GEOS-Chem v1.0, and BCC-AGCM-Chem.

	BCC-GEOS-Chem v2.0	BCC-GEOS-Chem v1.0	BCC-AGCM-Chem

Horizontal resolution	T42 (~2.8° × 2.8°)		
Vertical levels	L26 (up to 2.914 hPa) [a]		
High resolution capability	Available (T159L72) [b]	Unavailable	Unavailable
Chemistry	GEOS-Chem v14.0.1	GEOS-Chem v11-02b	MOZART2
Advected species	220	78	79
Chemical reactions	914	426	168
Emissions	HEMCO module	Hard-coded	Hard-coded
Radiative and cloud feedback	Available	Unavailable	Available
Interactive ocean and sea ice	Available	Unavailable	Available
Original model references	This work	Lu et al. (2020)	Wu et al. (2020)

[a] Approximately 8 levels in the troposphere and 18 levels in the stratosphere.

[b] The capability for BCC-GEOS-Chem v2.0 to be performed at high resolution has been developed. Results will be discussed in Section 6.

In addition, we perform sensitivity simulations with BCC-GEOS-Chem v2.0 to evaluate the feedback of aerosols on cloud properties and radiation (Table 2). The Base simulation represents the standard BCC-GEOS-Chem v2.0 simulation described above, which considers full aerosol-cloud-radiation interactions. Aerosol direct effect is simulated by linking aerosol optical properties (such as aerosol optical depth (AOD), single scattering albedo, and asymmetry factor) to the radiation scheme (Chapman et al 2009). The noARIs simulation inactivates the feedback of aerosol on radiation calculation. Aerosol indirect effect is simulated by linking prognostic aerosols to cloud condensation nuclei (CCN). In the noACIs simulation, we use a prescribed cloud droplet number concentration of 5 cm^{-3} to exclude aerosol indirect effect, following previous studies (Zhao et al., 2017; Zhang et al., 2018; Zhou et al., 2019; Sun et al., 2024). The noARIs and noACIs simulations are initialized in the year 2012, driven by the initial fields archived from the Base model, and model results in 2013 are compared with the Base simulation.

Table 2. Setup of sensitivity simulations compared with base simulation in BCC-GEOS-Chem v2.0

Experiment [a]	Base	noARIs [b]	noACIs [c]
Aerosol direct effect	on	off	on
Aerosol indirect effect	on	on	off

[a] The simulations are performed from 2012 to 2013, with the first year (2012) as model spin-up. [b] The noARIs simulation inactivates the feedback of aerosol on radiation calculation. [c] The noACIs simulation uses a prescribed cloud droplet number concentration of 5 cm^{-3} to exclude aerosol indirect effect.

3.2 Observations and reanalysis data used for model evaluation

We use ozonesonde, surface, and satellite observations, as well as the reanalysis data (Table S3), to evaluate the performance of the BCC-GEOS-Chem v2.0 simulation in representing atmospheric chemistry and climate parameters, with a focus on

SLCFs. Ozonesonde measurements are sourced from the World Ozone and Ultraviolet Radiation Data Centre (WOUDC), operated by the Meteorological Service of Canada within Environment and Climate Change Canada. Ozone from the surface to the stratosphere is measured by balloon-borne ozone electrochemical concentration cell instruments (Tarasick et al., 2019), with the sampling frequencies of 2-4 profiles per week. In this study, we use ozonesonde sites that meet the criteria outlined by Wang et al. (2022). In total, 16 sites across the globe are selected for model evaluation. We then categorize the WOUDC sites into 6 regions (Figure S2a).

Surface ozone observations are collected from individual national monitoring networks, covering major developed and developing regions in the northern hemisphere, including China, the United States of America (USA), Europe, South Korea, and Japan (Figure S2b). We applied data quality control measures to exclude unreliable data following Wang et al. (2024). Surface fine particulate matter ($PM_{2.5}$) data is derived from Shen et al. (2024), which estimates ground-level $PM_{2.5}$ for 2000-2019 by combining Aerosol Optical Depth (AOD) retrievals from multiple satellite products with the GEOS-Chem chemical transport model and a residual Convolutional Neural Network (CNN) technique.

Additionally, we use the OMI ozone profile (PROFOZ), which consists of 24 vertical layers extending from the surface to 60 km, as retrieved by Liu et al. (2010). This product has been validated through comprehensive comparisons with ozonesonde data (Huang et al., 2017) and other satellite products (Huang et al., 2018). We obtain total column ozone data from the Bodeker Scientific Filled Total Column Ozone database v3.4.1, and derive the vertical distribution of stratospheric ozone by ozone retrievals from Microwave Limb Sounder (MLS). We also incorporate the tropospheric nitrogen dioxide (NO_2) columns (Lamsal et al., 2021) and formaldehyde (CH_2O) column (De Smedt et al., 2015), with horizontal resolution of 0.25° × 0.25°. Other satellite observational datasets include carbon monoxide (CO) observations obtained from the Terra Measurement of Pollution in the Troposphere (MOPITT) satellite instruments (Deeter et al., 2021), and AOD at 550 nm from the Moderate Resolution Imaging Spectroradiometer (MODIS).

We also apply observations and reanalysis data to evaluate the performance of BCC-GEOS-Chem v2.0 on climate simulation and the aerosol's effect. The global monthly observations of radiative properties are obtained from Earth's Radiant Energy System (CERES) sensors onboard the Terra satellite (Kato et al., 2018), including shortwave and longwave cloud radiative forcings (SWCRF and LWCRF), downward shortwave (SWDOWN) radiation, and outgoing longwave radiation (OLR). The total precipitation is obtained from Global Precipitation Climatology Product (GPCP) satellite data (Huffman et al., 2001). The datasets for evaluation of surface temperature (TS), cloud fraction, and mass fraction of cloud liquid water are from the second version of Modern-Era Retrospective Analysis for Research and Applications (MERRA-2). Air temperature, zonal and meridional wind fields as well as the vertical velocity are obtained from the ERA5 reanalysis, which is provided by the European Centre for Medium-Range Weather Forecasts (ECMWF). Evaluations with these data show that BCC-GEOS-Chem v2.0 accurately reproduces tropospheric temperature, wind fields, radiation, cloud cover, and precipitation (Figure S3). However, it has limitations in simulating stratospheric circulations, which may contribute to stratosphere ozone biases, as will be detailed in Section 4.1. Consequently, biases in tropospheric compositions are more likely attributable to uncertainties in emission inventory and chemical mechanisms, which will be the focus of the following discussions. Nevertheless, we acknowledge that the potential contribution from meteorology to biases in tropospheric compositions cannot be ruled out.

4 Evaluation and intercomparison of modelled concentrations of short-lived climate forcers

4.1 Ozone

We present the spatial and seasonal distributions of global mid-tropospheric ozone derived from OMI satellite observations averaged over 2012–2014, and compare the discrepancies between these observations and the results from models in Figure 2. We analyse ozone at 700–400 hPa, where the OMI satellite has the peak sensitivity to ozone concentration (Liu et al., 2010). To ensure a proper comparison with observations, OMI averaging kernels and a priori profiles are applied to all model results following Zhang et al. (2010).

Satellite observations indicate high mid-tropospheric ozone levels over the northern midlatitudes both in boreal spring (March-April-May, MAM) and summer (June-July-August, JJA), due to active stratosphere-troposphere exchange (STE) and high photochemical production (Cooper et al., 2014). Elevated ozone levels are witnessed over southern Africa in boreal autumn (September-October-November, SON), driven by intense biomass burning emissions (Sauvage et al., 2007; Figure S1). BCC-GEOS-Chem v2.0 captures well the spatial and seasonal distributions of tropospheric ozone observed from OMI satellite, with high spatial correlation coefficients of r=0.77-0.92 for different seasons (Figure S4). Compared with satellite observations, BCC-GEOS-Chem v2.0 exhibits overall small global mean biases of mid-tropospheric ozone concentrations, ranging from -2.1 to 1.8 ppbv. Compared with BCC-GEOS-Chem v1.0, BCC-GEOS-Chem v2.0 slightly reduces the ozone low-bias in the northern midlatitudes. However, the model tends to overestimate ozone in the mid-latitudes, especially in the Tibetan Plateau by 4-20 ppbv in boreal spring, which may be attributed to excessive STE as will be demonstrated in Section 4.3.

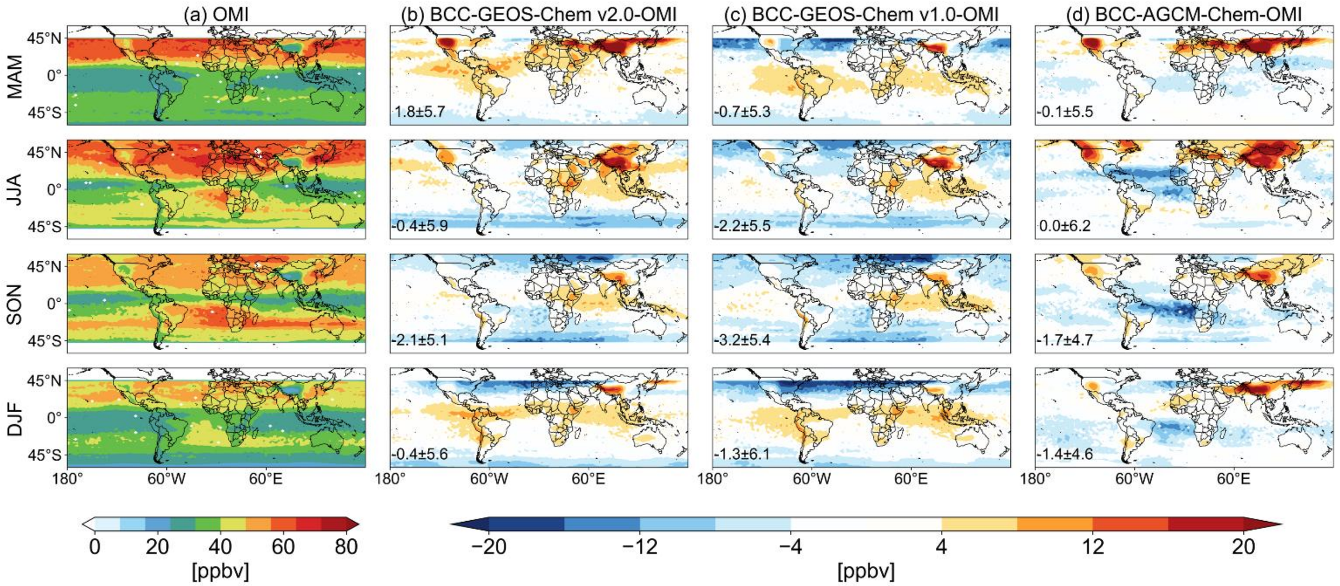

Figure 2. Spatial and seasonal distributions of global mid-tropospheric ozone averaged for 700-400hPa over 2012–2014 from (a) OMI satellite observation, (b) differences between BCC-GEOS-Chem v2.0 and OMI, (c) differences between BCC-GEOS-Chem v1.0 and OMI, and (d) differences between BCC-AGCM-Chem and OMI. All model outputs are applied with OMI averaging kernels for a proper comparison with the observations.

Figure 3 presents a comparative analysis of annual mean ozone vertical profiles simulated by BCC-GEOS-Chem v2.0, BCC-GEOS-Chem v1.0, and BCC-AGCM-Chem against WOUDC ozonesonde observations across six regions, averaged over the 2012-2014 period. The results demonstrate that both BCC-GEOS-Chem v2.0 and v1.0 effectively replicate observed ozone concentrations in the lower and middle troposphere (surface to 400 hPa), showing biases generally within 5 ppbv across most regions, except for an enhanced positive bias reaching 15 ppbv in tropical areas. In contrast, BCC-AGCM-Chem exhibits substantially larger positive biases of 8-20 ppbv throughout the lower and middle troposphere. This may be attributed to the better performance of BCC-GEOS-Chem in simulating the major precursors of tropospheric ozone, as will be demonstrated in Section 4.2.

Divergent model performance emerges in the upper troposphere and stratosphere. Both BCC-GEOS-Chem v2.0 and v1.0 successfully capture the abrupt ozone gradient transition in the upper troposphere-lower stratosphere (UTLS) region at tropics and mid latitudes region, demonstrating an excellent agreement with observed concentrations. BCC-GEOS-Chem v2.0 achieves superior representation of vertical ozone structure from the troposphere through the low stratosphere across tropics, Japan, Europe, and Canada, showing substantially reduced mean model biases (-21.2−1.6 ppbv at 400-200 hPa) compared with BCC-GEOS-Chem v1.0 and BCC-AGCM-Chem. However, both BCC-GEOS-Chem v2.0 and v1.0 tend to underestimate ozone levels in the Antarctic UTLS, while BCC-AGCM-Chem shows better agreement with observations as its chemical species are relaxed to prescribed monthly climatological values in the stratosphere instead of being simulated interactively.

Figure 4 compares the zonal mean stratospheric ozone distributions simulated by BCC-GEOS-Chem v2.0 and v1.0 with the MLS satellite observations. Overall, with the incorporation of the UCX scheme for interactive stratospheric chemistry, BCC-GEOS-Chem v2.0 captures the vertical ozone distribution of stratospheric ozone and replicates the ozone maximum between 30-5 hPa seen in the MLS observation. In contrast, BCC-GEOS-Chem v1.0 with a simplified linearized ozone parameterization simulates an anomalously broad ozone maximum and substantially underestimates its magnitude at 30-5 hPa compared to MLS. Furthermore, BCC-GEOS-Chem v2.0 better reproduces Antarctic stratospheric ozone depletion during austral spring than v1.0 (Figure S5), although the depletion remains less pronounced than observed. However, we also note that substantial biases persist in BCC-GEOS-Chem v2.0. We find an underestimation of 5-20% in upper-stratospheric ozone (30-4 hPa) relative to MLS, accompanied by a pronounced cold bias in upper-stratospheric temperature compared to ERA5 reanalysis data. Besides, BCC-GEOS-Chem v2.0 overestimates lower-to-middle stratospheric ozone (100-50 hPa) by over 50% compared to MLS, leading to an overestimation of the total column ozone (Figure S5c). In addition, while the model reproduces the overall vertical distribution of key stratospheric chemical component (e.g., NO_x, NO_y, methane), there are notable discrepancies in both the magnitude and location of concentration hotspots (Figure S6). These biases may be partly attributable to the model's limited top height in the T42L26 configuration. This constrains its ability to accurately simulate stratospheric circulations, and consequently, to reproduce the distributions and magnitudes of stratospheric chemical components that are significantly modulated by intense climate-chemistry interactions within the stratosphere (such as the interaction between stratospheric ozone and temperature). We find that although BCC-GEOS-Chem v2.0 captures the overall structure of the residual circulation (Figure S7), it underestimates the strength of the Brewer–Dobson circulation in the upper stratosphere over both the equatorial regions and high latitudes. This weaker tropical upwelling may partly account for high biases in lower-stratospheric ozone over the tropics. Our one-month high-resolution simulation using the T159L72 configuration indeed largely reduced the high ozone bias in the lower to middle stratosphere (Figure S8), highlighting the importance of an adequate model top and sufficient vertical resolution for simulating stratospheric ozone.

At the surface, however, all three models tend to overestimate surface ozone concentrations, which has been a long-standing issue among global chemical models (Gao et al., 2025). Figure 5 shows the scatter plots of the simulated and observed surface ozone concentrations over Europe, Asia, and the US over 2012-2014. We only use remote or rural sites here as a global model at a coarse resolution of ~2.8° is difficult to resolve pollutant levels at urban sites. BCC-GEOS-Chem v2.0 overestimates surface ozone levels, especially in Asia with high biases of 10-20 ppbv. These high biases are not prominent in BCC-GEOS-Chem v1.0 and other previous studies using earlier GEOS-Chem model versions (e.g., version 11). This discrepancy reflects complicated joint effects of the updated chemical mechanisms. For instance, the integration of updated aromatic chemistry in GEOS-Chem models from version 13.0.0 onwards elevates surface ozone concentrations by at least 5 ppbv in eastern China (Bates et al., 2021; Lu et al., 2025). Moreover, the removal of sea salt aerosol debromination in GEOS-Chem models from version 13.4.0 onwards, leading to an enhancement in ozone concentrations by up to 10 ppb especially over the Southern Ocean. Other significant updates in heterogeneous chemistry (e.g., updates in N_2O_5, NO_3, NO_2 reactive uptake, nitrate photolysis) can further modulate ozone concentrations through their impacts on ozone precursors. The larger ozone positive bias in BCC-GEOS-Chem v2.0 relative to BCC-GEOS-Chem v1.0 may also be attributed to the lower dry deposition velocity in the model, as will be discussed in Section 4.3. The representative issue when comparing model results with site measurements also emerges. Even though the comparisons are limited to rural or remote sites, the low resolution of these models (~200km) cannot resolve the heterogeneity of ozone precursors, thus leading to artificial mixing and biased ozone production efficiency (Wile and Prather, 2006; Yu et al., 2016; Young et al, 2018). In addition, these models are difficult to represent local meteorological conditions, particularly over complex terrain at such coarse resolution, further limiting their ability to capture site-level ozone concentrations. We will demonstrate in Section 6 that increasing the spatial resolution can significantly reduce the bias in simulated surface pollutant concentrations at site level.

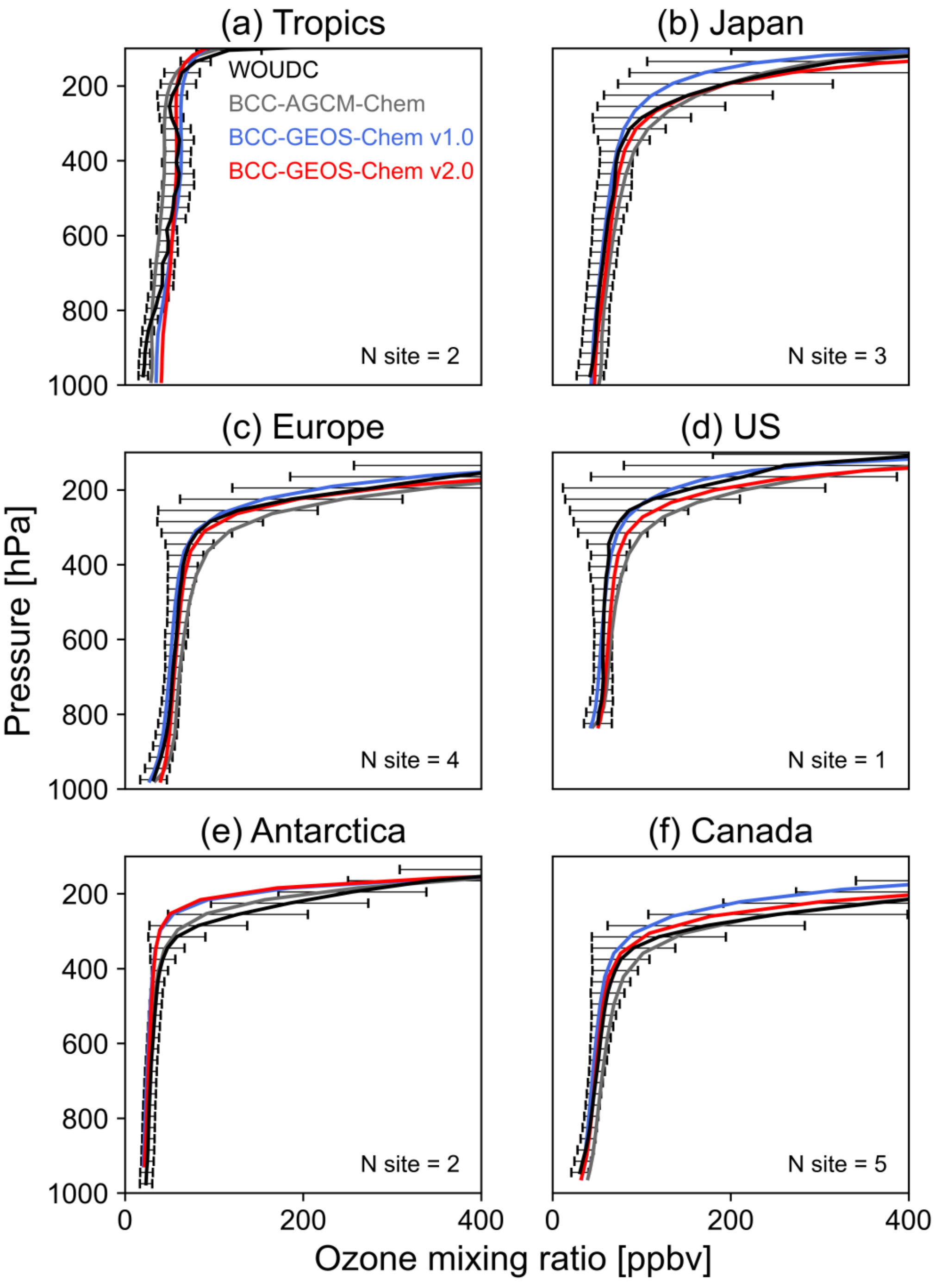

Figure 3. Comparisons of model simulated annual mean ozone vertical profiles to ozonesonde observations averaged over 2012-2014. Black solid line represents WOUDC observations, the others represent the model from BCC-AGCM-Chem, BCC-GEOS-Chem v1.0 and BCC-GEOS-Chem v2.0, respectively. Black horizontal bars are the standard deviations of WOUDC observations. Each panel represents the average of all sites in this region. Numbers of selected sites for each region in 2012–2014 are given.

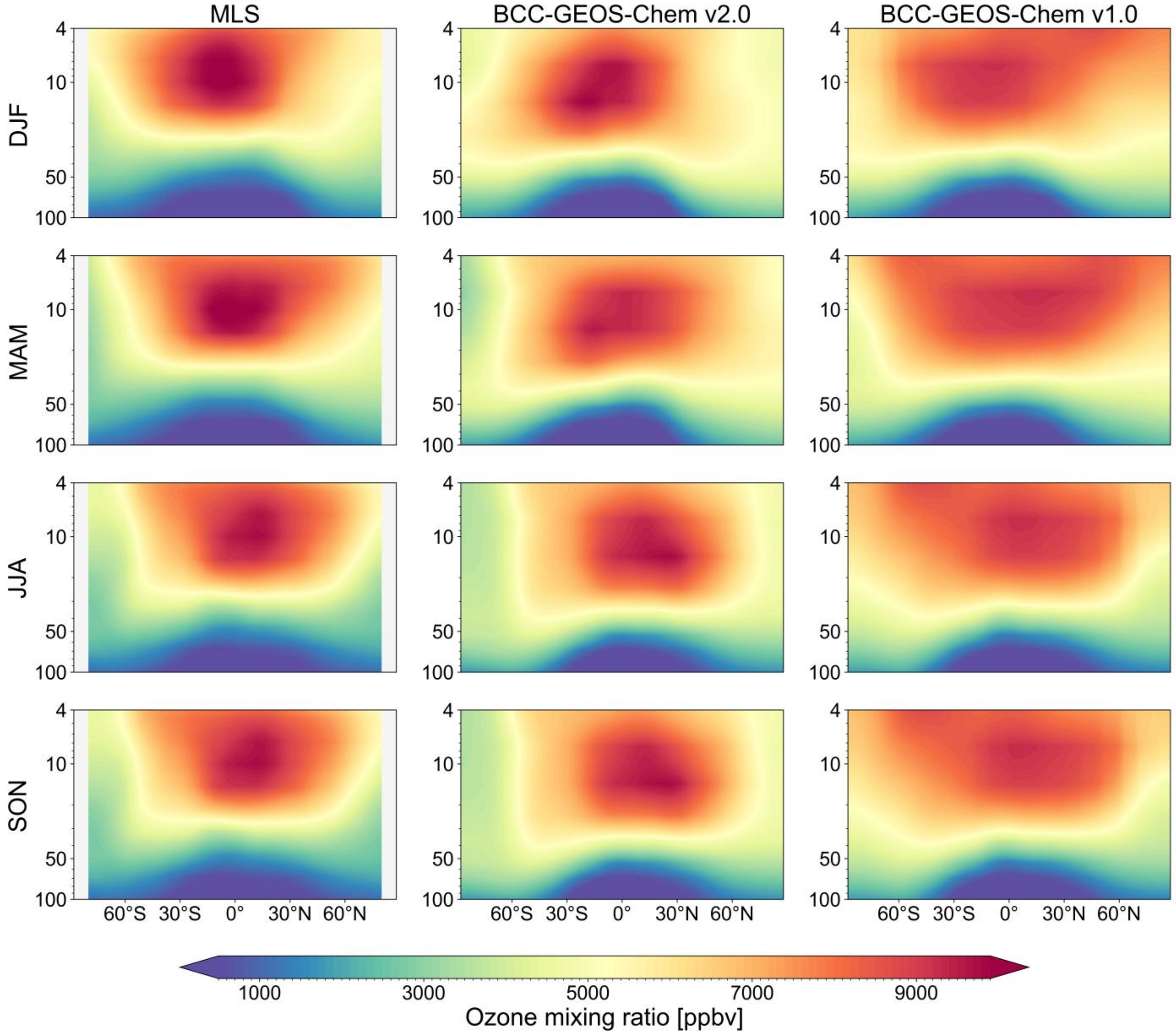

Figure 4. The zonal mean vertical and seasonal distributions of ozone in the stratosphere from BCC-GEOS-Chem v2.0 and BCC-GEOS-Chem v1.0 under T42L26 configuration and MLS. Values are averaged over 2012-2014.

530

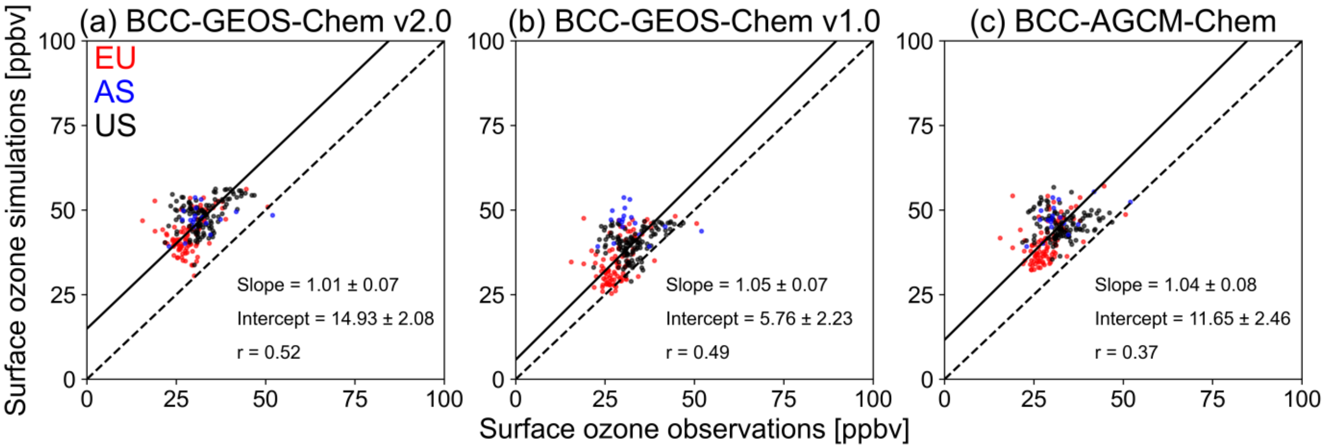

Figure 5. Scatter plots of observed and simulated surface ozone for (a) BCC-GEOS-Chem v2.0, (b)BCC-GEOS-Chem v1.0, and (c) BCC-AGCM-Chem over 2012-2014. The solid lines indicate the regression lines. The dotted lines indicate the 1: 1 line. Observations are averaged to the same model grid.

4.2 CH_2O, NO_2, CO, and aerosols

Comparison with satellite observations in Figure 6 demonstrate that BCC-GEOS-Chem v2.0 has significant improvements in simulating tropospheric CH_2O, NO_2, and CO. BCC-GEOS-Chem v2.0 shows a negative mean bias relative to OMI tropospheric CH_2O column of $-1.2\pm1.5\times10^{15}$ molecule cm^{-2} averaged over 2012-2014, with positive bias at the tropics. In comparison, both BCC-GEOS-Chem v1.0 and BCC-AGCM-Chem show positive bias of over 50% over the Amazon, central Africa, tropical Asia, and the southeastern United States. These two models show 10-50% larger BVOCs emissions over the hotspot regions compared to BCC-GEOS-Chem v2.0 despite comparable global total emissions (410 versus 389 Tg yr^{-1}), thereby partly explaining their high biases. In addition, the updated aromatic chemistry in BCC-GEOS-Chem v2.0 (GEOS-Chem version 13.0.0 onwards) further reduces simulated CH_2O over tropical regions such as central Africa and the Amazon (Bates et al., 2021). BCC-GEOS-Chem v2.0 also shows lower tropospheric CH_2O columns over the mid-latitudes in both hemispheres compared to OMI retrievals, consistent with the other two models. This pattern may be partly attributed to systematic uncertainties in satellite retrievals, as previous studies have shown that CH_2O retrievals are biased low on average by 20–51% relative to aircraft observations across mid-latitude regions (Zhu et al., 2016; Zhu et al., 2020).

For tropospheric NO_2, BCC-GEOS-Chem v2.0 shows no significant global mean bias compared to OMI tropospheric NO_2 column ($0.0\pm1.3\times10^{15}$ molecule cm^{-2}), but this reflects the compensation of negative bias over emission hotspots such as East Asia, India, Western Europe and central Africa, and positive bias over other regions. In comparison, the simulated tropospheric NO_2 column in BCC-GEOS-Chem v1.0 and BCC-AGCM-Chem shows substantially high positive biases of 4-7×10^{14} molecule cm^{-2} (55.4-107.3%) over continental regions, especially over East Asia and India. Given comparable surface NO_x emissions and consistent lightning NO_x parameterization across the three models, the improved performance in simulating tropospheric NO_2 columns is likely driven by differences in NO_x chemistry and nitrate aerosol treatments between the models. Compared to BCC-GEOS-Chem v1.0, BCC-GEOS-Chem v2.0 with up-to-date GEOS-Chem chemical mechanism has incorporated updated aromatic chemistry (GEOS-Chem version 13.0.0 onwards) and the reaction updates in NO_x chemistry. These updates reduce bias in simulated NO_2 column concentrations, as reported in CESM2-GC (Fritz et al., 2022). Besides, the absence of nitrate aerosol chemistry in BCC-AGCM-Chem (Wu et al., 2020) limits a realistic representation of the gas–particle partitioning of reactive nitrogen, thereby leading to the overestimation of tropospheric NO_2 column.

For CO, we evaluate simulated CO concentrations at 700 hPa, where the MOPITT satellite has generally high sensitivity (Emmons et al., 2004; Pfister et al., 2005). BCC-GEOS-Chem v2.0 has also substantially reduced the positive bias relative to observed values, averaged 4.9±11.9 ppbv (5.5%) over the globe, compared with the excessive positive CO bias of BCC-GEOS-Chem v1.0 (24.8±12.9 ppbv) and BCC-AGCM-Chem (50.8±14.1 ppbv) with even larger bias over Asia, central Africa, and the East Pacific Ocean. The excessive CO concentrations in BCC-AGCM-Chem are primarily attributable to a severely underestimated atmospheric oxidizing capacity, with the global column-weighted mean OH concentration being nearly 50% lower than that in BCC-GEOS-Chem v2.0 (0.5×10^6 molecule cm^{-3} versus 1.0×10^6 molecule cm^{-3}), in addition to higher biomass burning and anthropogenic emissions (1140 Tg yr^{-1} versus 925 Tg yr^{-1}; Table S1).

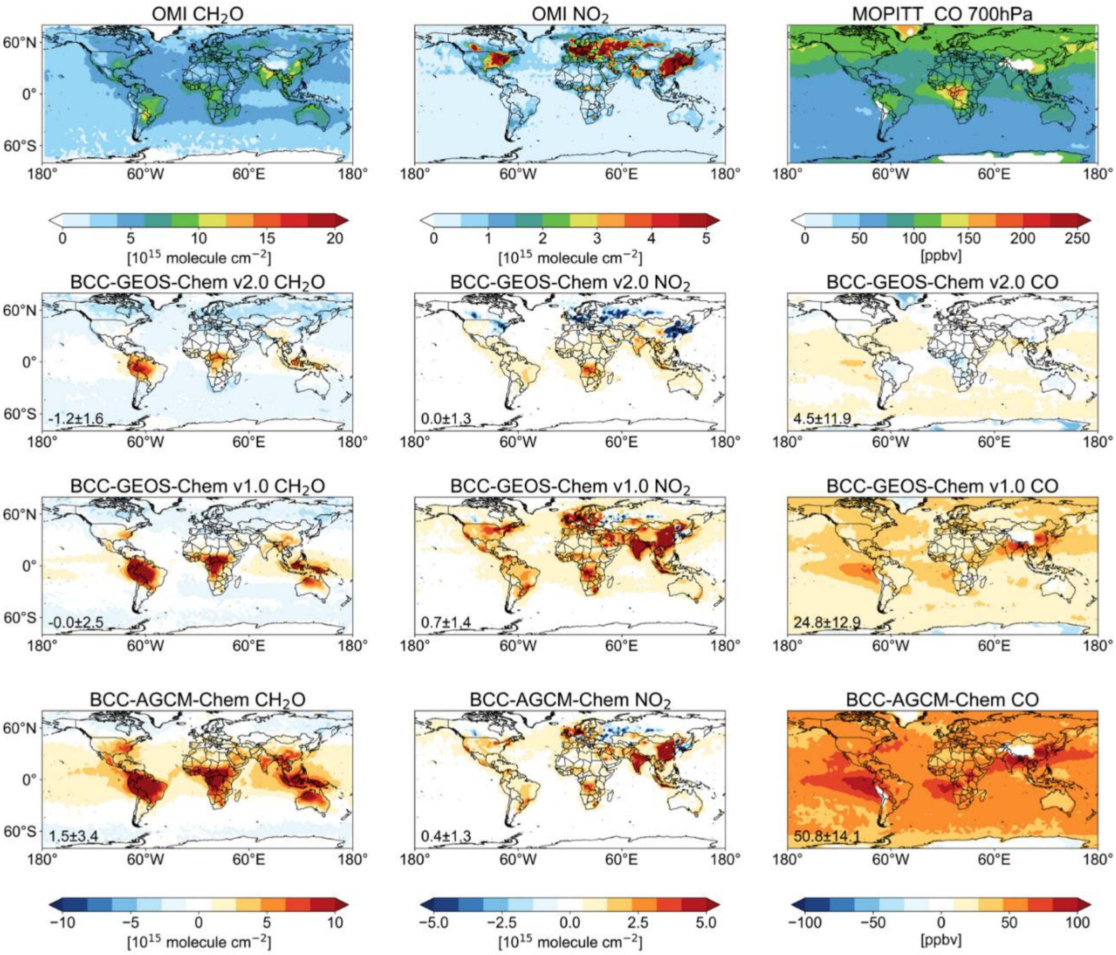

Figure 6. Spatial distributions of global tropospheric NO₂ column averaged over 2012–2014 from (a) OMI satellite observation, (b) differences between BCC-GEOS-Chem v2.0 and OMI, (c) differences between BCC-GEOS-Chem v1.0 and OMI, and (d) differences between BCC-AGCM-Chem and OMI.

Figure 7 evaluates the simulated surface fine particulate matter ($PM_{2.5}$) concentrations with the satellite-derived data as introduced in Section 3.2 (Shen et al., 2024). The satellite-derived data reveal high $PM_{2.5}$ concentration over East Asia and India due to intensive anthropogenic emissions, and over northern and central Africa due to mineral dust and biomass burning emissions. BCC-GEOS-Chem v2.0 reproduces the overall spatial distributions and magnitude of observed $PM_{2.5}$ concentrations, though it tends to marginally underestimate concentrations in the hotspot regions (e.g., Amazon, central Africa, and India), which is most likely due to the coarse model resolution and the uncertainties of biomass burning (Reddington et al., 2017). BCC-GEOS-Chem v2.0 demonstrates superior performance in simulating $PM_{2.5}$ concentration compared with BCC-GEOS-Chem v1.0, which exhibits pronounced overestimation in East Asia, India, the Arabian

Peninsula, and Northern Africa, and BCC-AGCM-Chem, which significantly underestimates $PM_{2.5}$ concentrations in major emission hotspot regions. This improvement is likely due to its better performance in simulating the gas-phase precursors as shown above (Figure 6). The large negative bias in BCC-AGCM-Chem is mainly due to the absence of nitrate aerosol chemistry and the incomplete representation of secondary organic aerosol formation (Wu et al., 2020).

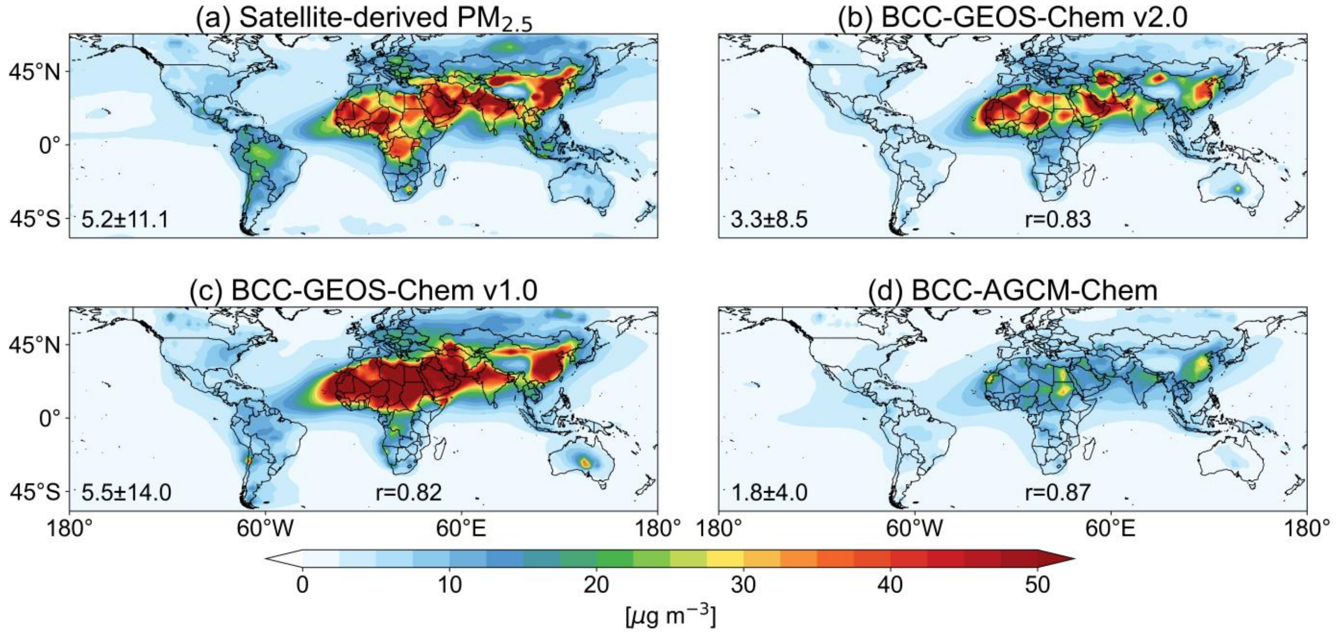

Figure 7. Spatial distributions of annual mean Surface fine particulate matter ($PM_{2.5}$) from (a) Satellite-derived $PM_{2.5}$, (b) BCC-GEOS-Chem v2.0, (c) BCC-GEOS-Chem v1.0, and (d) BCC-AGCM-Chem. Values are averaged over 2012-2014.

4.3 Diagnostics of tropospheric ozone budgets and OH concentrations

We then diagnose the global tropospheric ozone budget and tropospheric oxidation capacity (using global air-mass-weighted tropospheric OH and methane lifetime against tropospheric OH loss as key metrics) in BCC-GEOS-Chem v2.0, and compared these results with those from BCC-GEOS-Chem v1.0 and other studies in the literature (Table 4). The results from BCC-AGCM-Chem are not presented here, as its diagnostics for O_x production and loss are not available.

The global tropospheric ozone burden simulated by BCC-GEOS-Chem v2.0 is 355 Tg averaged over 2012-2014, about 5.7% higher than the result from BCC-GEOS-Chem v1.0 and falls within the range (250-410 Tg) estimated by ~50 models assessments from Young et al. (2018). The global tropospheric mean OH concentration in BCC-GEOS-Chem v2.0 is smaller than that from BCC-GEOS-Chem v1.0 (0.97×10^6 vs. 1.16×10^6 molecule cm^{-3}) and falls within the range (0.74–1.33×10^6 molecule cm^{-3}) estimated from multiple chemical models (Naik et al., 2013). Table 3 further compares the simulated air-mass-weighted tropospheric mean OH with the observation-based results from Zhao et al. (2023) across different latitudinal bands. The observation-based OH concentrations are estimated by adjusting simulated OH precursors and meteorological conditions to the observations in chemical box models. We find that the overall latitudinal distributions of OH in BCC-GEOS-Chem v2.0 align with observation-based results with biases below 2×10^5 molecule cm^{-3}, whereas BCC-GEOS-Chem v1.0 has a substantial high bias, especially in the tropics (3.9-4.8×10^5 molecule cm^{-3}). Discrepancies in meteorological conditions and concentrations of methane, ozone, NO_x, and CO can all contribute to the OH bias in climate–chemistry models (Nicely et al., 2020). The derived methane chemical lifetime against OH loss is 9.28 years in BCC-GEOS-Chem v2.0, which falls in the middle range reported from multi-model assessments (7.1-14.0 years) (Naik et al., 2013).

We further examine the diagnostics of the chemical production and loss of the odd oxygen (O_x) family, which includes O_3, NO_2, NO_y, several organic nitrates, and halogen species (a total of 67 species in GEOS-Chem v14.0.1) to account for rapid cycling between O_x components. Ozone accounts for over 95% of total O_x according to Hu et al. (2017). The global annual ozone chemical production and loss are 6356 and 6272 Tg, respectively. These estimates of O_x chemical production and loss are higher than results in BCC-GEOS-Chem v1.0 but still fall in the range from ~30 models assessments presented by Young et al. (2018). However, we find that the difference between the estimated O_x chemical production and loss (~100 Tg) is much smaller than the multi-model estimate (~500 Tg) (Table 4). GEOS-Chem "Classic" version 14.0.0 driven by reanalysis meteorology fields also yields a relatively small difference between the O_x chemical production and loss of 377 Tg (https://ftp.as.harvard.edu/gcgrid/geos-chem/1yr_benchmarks/). The production to loss difference between the BCC-GEOS-Chem v2.0 and multi-model estimates in Young et al. (2018) may be partly attributed to the discrepancies in the metric (O_x vs ozone), but is more likely due to the difference in the chemical scheme.

The global annual mean ozone dry deposition flux simulated by BCC-GEOS-Chem v2.0 is 1061 Tg averaged over 2012-2014, which shows agreement in the results of BCC-GEOS-Chem v1.0 and falls within the range (700-1500Tg) estimated by Young et al. (2018). Figure 8 illustrates the annual mean distribution of global ozone dry deposition velocity over 2012–2014, as simulated by BCC-GEOS-Chem v2.0, BCC-GEOS-Chem v1.0, and BCC-AGCM-Chem. The overall spatial distribution of ozone dry deposition velocity in BCC-GEOS-Chem v2.0 is similar to that in BCC-GEOS-Chem v1.0, but the values are slightly slower. This is attributed to two reasons. First, as introduced in Section 2.3.3, BCC-GEOS-Chem v2.0 utilizes offline Olson map land types and LAI data to replace those from the BCC-AVIM. In contrast, BCC-GEOS-Chem v1.0 uses land types and leaf area indices information diagnosed from the BCC-AVIM. Second, the BCC-GEOS-Chem v2.0 has included the new deposition scheme over oceans (Pound et al., 2020). The new scheme has been shown to reduce the area-weighted mean ozone deposition over ocean by 50%, and the global total deposition flux by 17% (Pound et al., 2020). However, the total ozone dry deposition flux in BCC-GEOS-Chem v2.0 is 20% higher than that in BCC-GEOS-Chem v1.0, due to the higher surface ozone concentration. In comparison, the BCC-AGCM-Chem applies the archived ozone dry deposition velocity from the MOZART simulation (Wu et al., 2020), which is likely too small compared with observations.

We estimate the annual STE of ozone as 977 Tg in BCC-GEOS-Chem v2.0, calculated as the residual of the mass balance among tropospheric chemical production, chemical loss, and deposition. This is higher than the high end of the range from multi-model estimates (180-920 Tg) in Young et al. (2018). The estimate of BCC-GEOS-Chem v1.0 (336 Tg) was considered too small and caused the ozone underestimates in the upper troposphere (Figure 3), primarily due to the lack of representation in stratospheric chemistry (Lu et al., 2020). However, the inclusion of UCX in BCC-GEOS-Chem v2.0 seems to over-correct this issue. Figure 3 shows that in the UTLS regions, BCC-GEOS-Chem v2.0 agrees well with the ozonesonde observations in the tropics, East Asia, Canada, and Europe, while shows high ozone bias in the US and low bias in the Antarctica. However, we do find that BCC-GEOS-Chem v2.0 overestimates lower-to-middle stratospheric ozone (100-50 hPa) by over 50% compared to MLS (Figure 4) Biases in the simulated the Brewer–Dobson circulation as discussed in Section 4.1 can also contribute to the high STE flux. The STE diagnosed from the mass balance method may also be biased, as it is not a direct diagnostic of the dynamic flux between the stratosphere and the troposphere. More work is required to address this issue.

Table 3. The simulated and observation-based OH (in 10^5 molecule cm^{-3}) averaged over latitudinal bands.

	90-30° S	30-0° S	0-30° N	30-90° N
Observation-based [a]	5.3	12.2	14.5	7.2
BCC-GEOS-Chem v2.0	4.6	12.1	12.7	6.0
BCC-GEOS-Chem v1.0	7.0	17.0	18.4	9.0

[a] From Zhao et al. (2023) simulations in CESM constrained by observations.

Table 4. Global Budget Diagnostics of Tropospheric Ozone in BCC-GEOS-Chem v2.0

Diagnostic term related to tropospheric ozone	BCC-GEOS-Chem v2.0 (this study)	BCC-GEOS-Chem v1.0[a] (Lu et al., 2020)	References
Ozone burden (Tg)	355	336	Mean: 340; range: 250–410[b]
O_x chemical production (Tg yr^{-1}) [c]	6356	5486	Mean: 4900; range: 3800–6900[d]
O_x chemical loss (Tg yr^{-1}) [c]	6272	4983	Mean: 4600; range: 3300–6600[d]
Dry deposition (Tg yr^{-1})	1061	873	Mean: 1000; range: 700–1500[d]
Global OH (10^6 molecule cm^{-3}) [e]	0.97	1.16	Mean: 1.11; range: 0.74–1.33[f]
Methane chemical lifetime (yr)	9.28	8.27	Mean: 9.7; range: 7.1-14.0[f]
STE (Tg yr^{-1}) [g]	977	370	Mean: 500; range: 180–920[d]

[a] From Lu et al. (2020) results in BCC-GEOS-Chem v1.0, the version of GEOS-Chem was v11-02. [b] Based on Figure 3 in Young et al. (2018), the ensemble burden represents ~50 models for year 2000 conditions. [c] Budget pertains to the odd oxygen (O_x) family, which includes O_3, NO_2, NO_y, several organic nitrates, and halogen species (a total of 67 species in GEOS-Chem v14.0.1). Ozone constitutes more than 95% of the total O_x. [d] From Figure 3 in Young et al. (2018), the ensemble fluxes represent ~30 models for year 2000 conditions. [e] Global annual mean air mass weighted OH concentration in the troposphere. [f] From Table 1 in Naik et al. (2013), the budget is based on an ensemble of 16 models for year 2000 conditions. [g] Estimated from the residual of mass balance among tropospheric chemical production, chemical loss, and deposition.

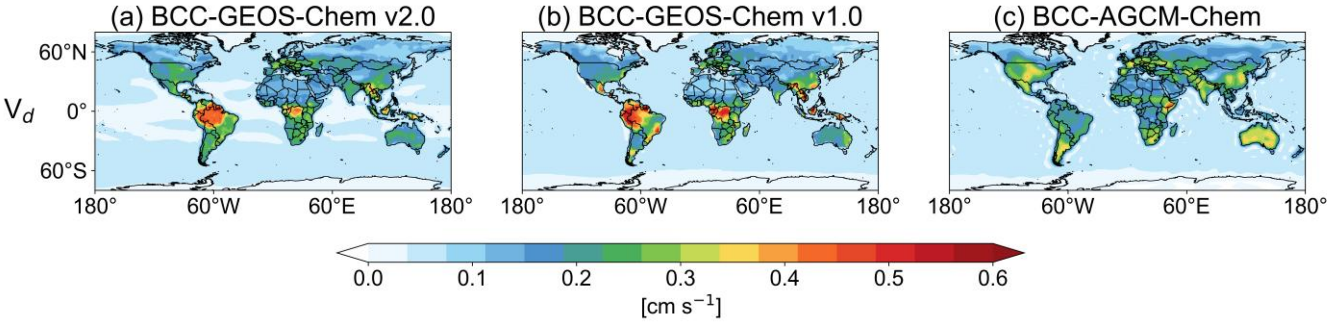

Figure 8. Annual mean distribution of global ozone dry deposition velocity for 2012–2014 from (a) BCC-GEOS-Chem v2.0, (b) BCC-GEOS-Chem v1.0, and (c) BCC-AGCM-Chem.

5 Influence of aerosols on radiation and clouds in BCC-GEOS-Chem v2.0

In this section, we evaluate the capability of the BCC-GEOS-Chem v2.0 model to simulate key metrics describing climate conditions, and quantify the contributions of atmospheric aerosols to these metrics as a means to assess the implementation of aerosol feedback in the model. These metrics to be examined include surface temperature (TS), precipitation, radiative and cloud properties such as downward shortwave (SWDOWN) radiation, outgoing longwave radiation (OLR), shortwave and longwave cloud radiative forcing (SWCRF and LWCRF), cloud fraction, cloud droplet number concentration, and cloud liquid water. Model performance is evaluated through comparisons with satellite observations and MERRA-2 reanalysis data (Table S3). Results are summarized in Figures 9–10 and Table 5.

Global annual mean surface temperature in BCC-GEOS-Chem v2.0 is 288.5 K, slightly higher than 287.1 K in MERRA-2 reanalysis data averaged over 2012-2014. BCC-GEOS-Chem v2.0 also demonstrates robust performance in simulating radiative fluxes and cloud properties, with consistent spatial distributions and no significant bias compared with observations or reanalysis data. The simulated global annual mean SWDOWN and OLR show general agreement with CERES data (153.9 vs. 164 W m^{-2} for SWDOWN and 217.3 vs. 224.9 W m^{-2} for OLR, respectively), with high spatial correlation coefficients (r) exceeding 0.96 between the simulation and CERES data. The model also reproduces the MERRA-2 global annual mean CF (0.65 vs. 0.65) and its spatial distribution (r=0.66). Simulated total precipitation also aligns with GPCP data (2.33 vs. 2.24 mm day^{-1}) with a spatial correlation coefficient of 0.83. A slightly larger bias is found for cloud radiative forcing. The simulated SWCRF underestimates CERES observations by 9.8 W m^{-2} (-39.8 vs. -49.2 W m^{-2}), while LWCRF is overestimated by 3.8 W m^{-2} (26.4 vs. 22.6 W m^{-2}). The cloud liquid water mass fraction shows excellent agreement with MERRA-2 reanalysis data (5.92×10^{-6} vs. 5.95×10^{-6} kg kg^{-1}).

The BCC-GEOS-Chem v2.0 model is able to reproduce the aerosols' impact on radiative budget, e.g., decreasing SWDOWN, OLR, and LWCRF, and increasing SWCRF (Table 5), as reported in literatures (e.g., Pendharkar et al., 2023). Sensitivity simulations further quantify the impact of ARIs and ACIs on the radiation (Figure 9 c and d). ARIs and ACIs lead to changes in SWDOWN of -3.3 and -14.1 W m^{-2}, respectively. The spatial heterogeneity in ARI-induced changes in SWDOWN is mainly attributed to the absorbing characteristics of aerosols and their semi-direct effects on cloud droplet evaporation. The impact of ACIs on SWDOWN is mainly driven by clouds activated by aerosols, leading to a greater scattering of shortwave radiation. These results are consistent with regional model studies across Asia and Africa (Feng et al., 2021; Feng et al., 2025) and global climate model studies (Wang et al., 2021; Zhao et al., 2022). For OLR, we find that ARIs decrease the global mean value by 0.6 W m^{-2} but with a mild increase in tropical regions where absorbing aerosols are higher, while ACIs substantially decrease by OLR by 9.7 W m^{-2}, largely attributable to its impact on high clouds. In addition, the model estimates that ACIs amplify SWCRF by 14.6 W m^{-2} while decreasing LWCRF by 1.3 W m^{-2}, showing higher impacts than ARIs. These tendencies are consistent with reported aerosols' feedback on cloud radiative forcing (Pendharkar et al., 2023).

Figure 10c and d further quantify the impact of aerosols on cloud properties and total precipitation through ACIs and ARIs from BCC-GEOS-Chem v2.0. For the global average, ACIs promote cloud development but suppress precipitation, as evident in an increase of 0.2% in cloud fraction and 21.7% in cloud liquid water but a decrease of 16.3% in total precipitation in the BASE simulation compared with the noACIs simulation (Table 5). The increases in cloud fraction and cloud liquid water are notable in the middle and high latitudes, while the influences on precipitation are mostly concentrated in the tropics, consistent with other modelling studies (e.g., Zelinka et al., 2014; Pendharkar et al., 2003). These results reflect the Twomey effect (Twomey 1977), i.e., aerosols are activated as cloud condensation nuclei (CCN), more but smaller cloud droplets are activated. With the reduction of the effective radius of cloud droplets, the collision-coalescence processes are hindered, and the precipitation of cloud water is delayed (Rosenfeld et al., 2008). Our simulations thus suggest reasonable feedback of aerosol indirect effect in BCC-GEOS-Chem v2.0. In comparison, the impact of ARIs on cloud properties and precipitation is rather small.

Table 5. Comparison of the radiative and cloud properties between observations and simulations.

Variable	Observation/Reanalysis	Base	noARIs	noACIs
SWDOWN	164.0	153.9	157.2	168.0
TS	287.1	288.5	289.1	293.5

OLR	224.9	217.3	217.9	227.0
SWCRF	-39.8	-49.2	-51.1	-34.6
LWCRF	22.6	26.4	26.5	27.7
CF	0.65	0.65	0.65	0.65
CDNC	/	69	69	5(fixed)
CLW (10^{-6})	5.92	5.95	5.99	4.66
PREP	2.24	2.33	2.36	2.71

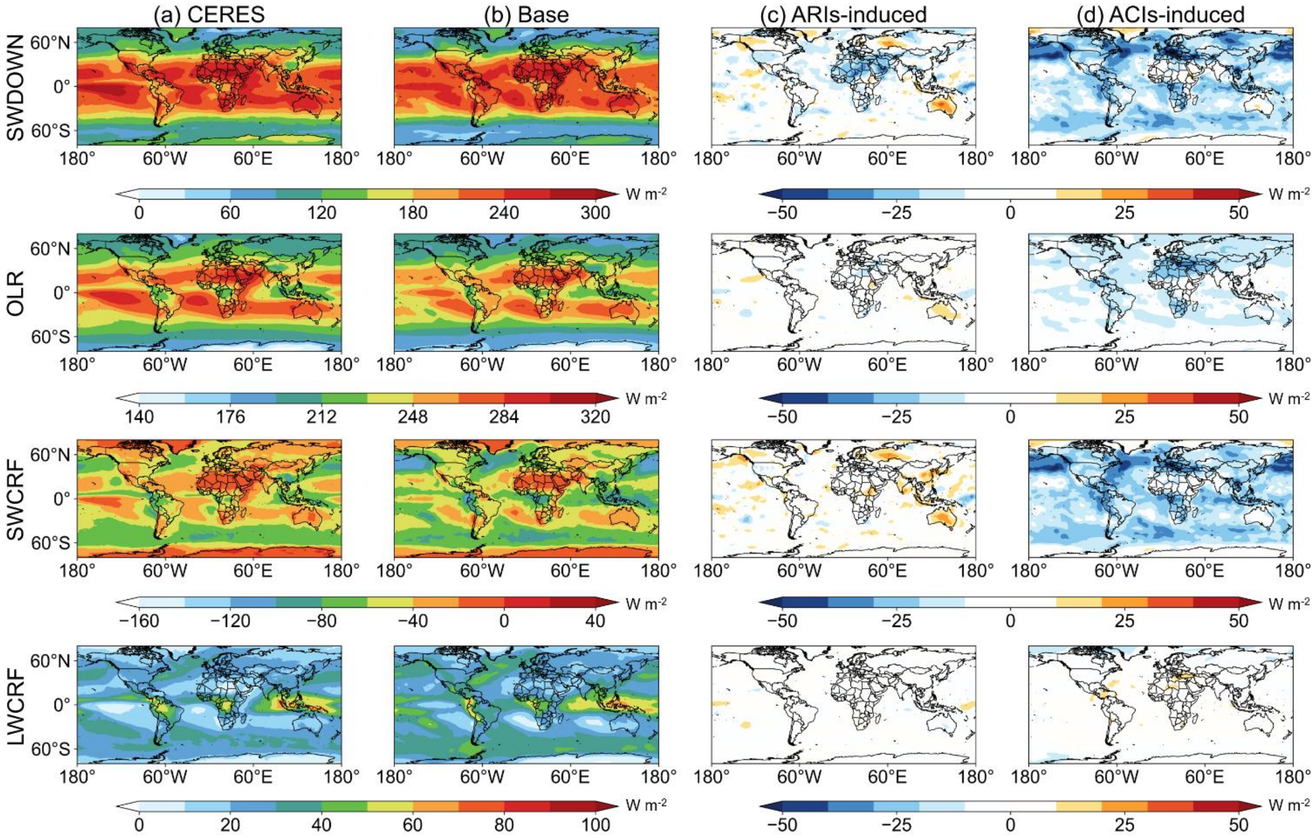

Figure 9. Annual mean radiative properties from (a) CERES satellite observations, (b) Base simulation, (c) ARIs-induced, and (d) ACIs-induced. Variables evaluated include the downward shortwave (SWDOWN) radiation, shortwave cloud radiative forcing (SWCRF), longwave cloud radiative forcing (LWCRF), and outgoing longwave radiation (OLR).

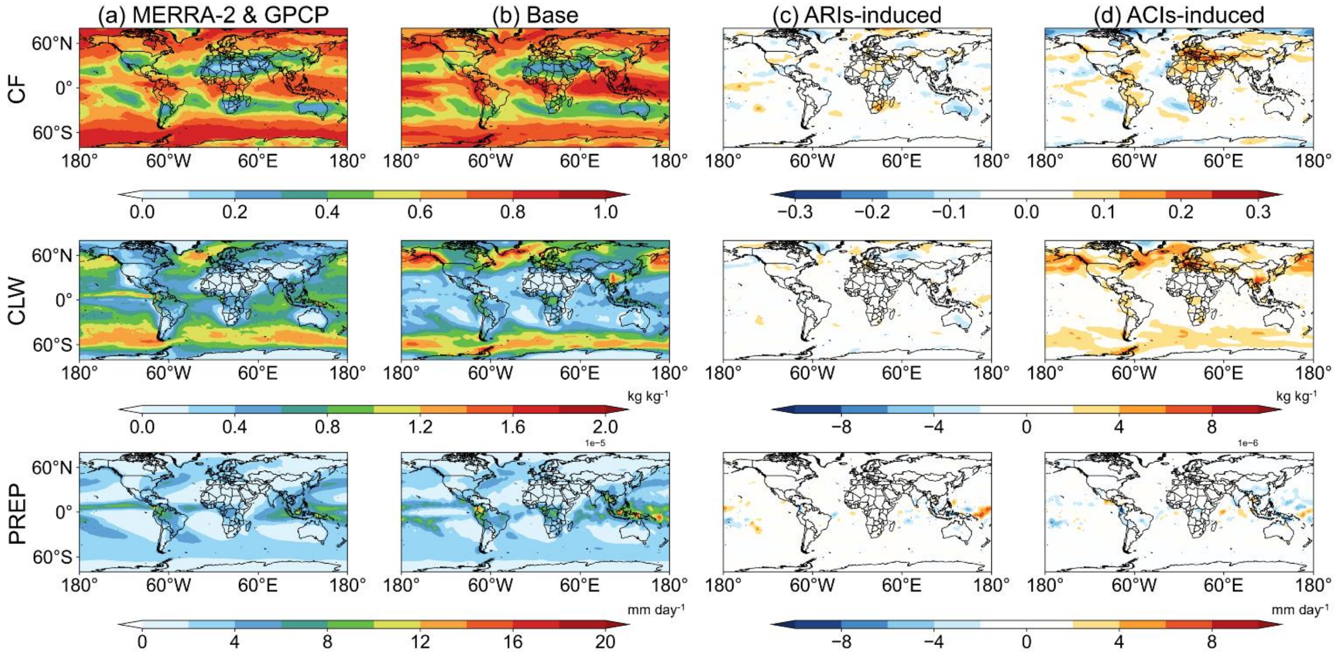

Figure 10. Annual mean cloud properties from (a) MERRA-2 reanalysis data or GPCP satellite data, (b) Base simulation, (c) ARIs-induced, and (d) ACIs-induced. Variables evaluated include the cloud fraction (CF), mass fraction of cloud liquid water (CLW), and total precipitation (PREP).

6 High-resolution simulation capability in BCC-GEOS-Chem v2.0: comparison of one-month simulation between T42L26 and T159L72

Our analysis above has demonstrated the capability of BCC-GEOS-Chem v2.0 in simulating atmospheric chemistry and climate at T42L26 resolution. In this section, we evaluate the high-resolution (T159L72) configuration of BCC-GEOS-Chem v2.0, with approximately 0.75° latitude × 0.75° longitude for horizontal resolution and with 72 vertical hybrid layers extending from the surface to 0.01 hPa. This further utilizes the grid-independent coupling capability of BCC-GEOS-Chem, enabling seamless integration of the GEOS-Chem chemical module with ESMs across customizable grid configurations and spatial resolutions. As such, the chemical module in BCC-GEOS-Chem v2.0 for the two configurations is exactly the same. The differences in timestep and pressure level between T42L26 and T159L72 are shown in Table S4 and S5. The T159L72 simulation was constrained to a one-month testing period (January 2014) due to the substantial computational cost escalation, which demands approximately 104 times more computational resources than the T42L26 simulation.

Figure 11 compares the spatial distributions of global atmospheric CO concentrations at 700 hPa and surface NO_2, ozone, and $PM_{2.5}$ concentrations in China from the BCC-GEOS-Chem v2.0 simulation at T159L72 versus T42L26 resolution.

Comparison of CO concentrations at 700 hPa aims to demonstrate the differences in transport of trace gases in the free troposphere between the simulations at the two resolutions. As expected, the T159L72 configuration demonstrates markedly enhanced capability in resolving fine-scale CO plume transport dynamics, particularly pronounced over African and Indonesian source regions, whereas the corresponding coarse-resolution T42L26 simulation fails to reproduce these persistent plumes due to rapid dissipation by numerical diffusion (Eastham et al., 2017; Zhuang et al., 2018) (Figure 11a and b). These results highlight the advantage of high-resolution simulation in mitigating numerical diffusion in Eulerian models.

Comparison of surface NO_2, ozone, and $PM_{2.5}$ concentrations aims to reveal the distinct resolution-dependent characteristics in pollution patterns. We thus focus on China where air pollutions were severe in January 2014. For surface $PM_{2.5}$ and NO_2 concentrations, the T159L72 configuration successfully resolves concentrated pollution hotspots over eastern China (Figure 11d, f, and h). In contrast, the coarser T42L26 model significantly attenuates these peak values through excessive spatial smoothing (Fig 10c, e, and g). This disparity arises from the inability of the model at coarse resolution to resolve fine-scale emission features from the inventory data, coupled with artificial mixing artifacts inherent to large grid-cell discretization. For surface ozone simulations, the T159L72 configuration produces higher ozone concentrations across most regions compared with the coarser T42L26 simulation, while showing lower ozone levels over the North China Plain. This is attributable to the unique photochemical regime in wintertime North China, where substantial NO_x emissions drive ozone formation into a VOC-limited regime. The intensified NO_x titration effect under such chemical conditions effectively suppresses ozone accumulation, a process that the high-resolution model better represents through refined precursor gradient resolution. Comparison of the simulated surface $PM_{2.5}$, NO_2, and ozone concentrations with the surface monitoring network of air quality in China (Figure 11) supports that the T159L72 simulation shows higher spatial correlation coefficients (r=0.40-0.55) with the observed values and substantially reduces the mean biases (MB) across all sites (expect for ozone) compared to the T42L26 simulation. In summary, the high-resolution implementation of BCC-GEOS-Chem v2.0 highlights the advantages and enhanced flexibility of our BCC-GC-HEMCO interface, and shows attractive potential for future applications in air quality simulation.

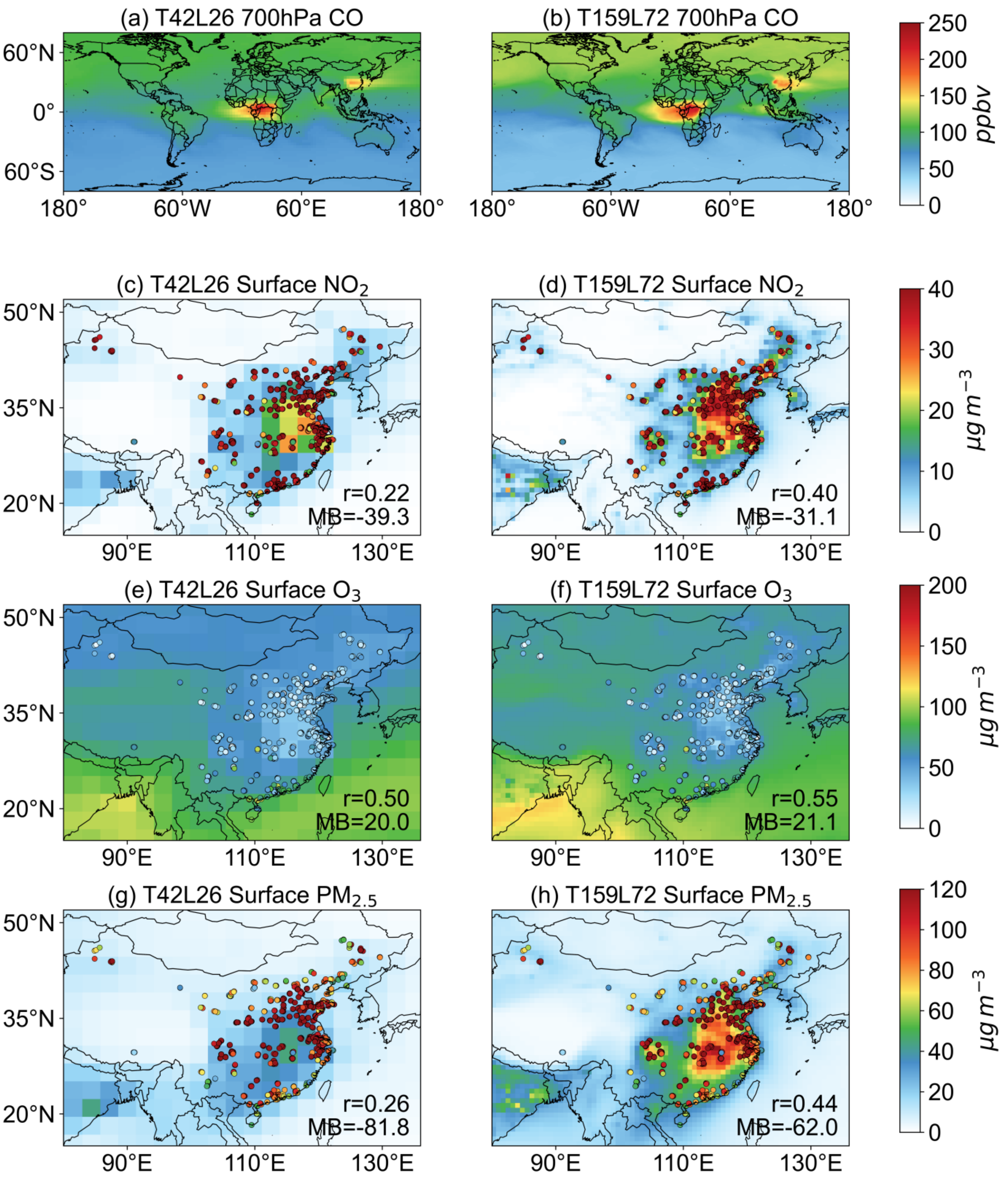(a) T42L26 700hPa CO
(b) T159L72 700hPa CO
60°N
0°
60°S
180°
60°W
60°E
180°
250
200
150
100
50
0
ppbv
(c) T42L26 Surface NO$_2$
(d) T159L72 Surface NO$_2$
50°N
35°N
20°N
90°E
110°E
130°E
r=0.22
MB=-39.3
r=0.40
MB=-31.1
40
30
20
10
0
μg m^{-3}
(e) T42L26 Surface O$_3$
(f) T159L72 Surface O$_3$
r=0.50
MB=20.0
r=0.55
MB=21.1
200
150
100
50
0
μg m^{-3}
(g) T42L26 Surface PM$_{2.5}$
(h) T159L72 Surface PM$_{2.5}$
r=0.26
MB=-81.8
r=0.44
MB=-62.0
120
100
80
60
40
20
0
μg m^{-3}

Figure 11. Spatial distributions of BCC-GEOS-Chem v2.0 simulated global 700hPa CO, and surface NO_2, surface O_3, and surface $PM_{2.5}$ in China at the resolution of T42L26 and T159L72 in January 2014. Mean bias (MB) and spatial correlation coefficients between the simulated and observed values are shown inset.

7 Summary and future plans

We have developed the BCC-GEOS-Chem v2.0, an online two-way chemistry-climate coupled model that incorporates feedback from chemically reactive greenhouse gases and aerosols. BCC-GEOS-Chem v2.0 has evolved into a fully coupled Earth system model that integrates the modules including the atmospheric component BCC-AGCM, the land component BCC-AVIM, the oceanic component MOM, and the sea ice component SIS. The standard chemical mechanism in the BCC-GEOS-Chem v2.0 features a comprehensive O_x-NO_x-VOC-halogen-aerosol chemistry in the unified tropospheric–stratospheric chemistry extension (UCX) scheme. The BCC-GC-HEMCO interface serves as a nexus linking the atmospheric module, an independent HEMCO emission module, and the GEOS-Chem chemical module.

We use satellite, ozonesonde, and surface observations to evaluate the performance of the BCC-GEOS-Chem v2.0 simulation at T42L26 (2.8°× 2.8° and 26 vertical layers with a top at 2.914 hPa) resolution in representing atmospheric chemistry, and compare with the model outputs from the BCC-GEOS-Chem v1.0 and BCC-AGCM-Chem for the same simulated time period (2012–2014). Results demonstrate that BCC-GEOS-Chem v2.0 captures well the main spatial and seasonal distributions of tropospheric ozone observed by multiple instruments, and also shows improved performance in simulating major gaseous pollutants and surface $PM_{2.5}$ compared with the BCC-GEOS-Chem v1.0 and BCC-AGCM-Chem. The diagnostics of tropospheric ozone budgets and OH concentrations generally agree with the observation-constrained values and multi-model assessment. However, the model derives a relative low value of the difference between tropospheric ozone chemical production and loss and shows a high STE flux that requires further investigation.

BCC-GEOS-Chem v2.0 is now able to consider aerosol-climate interactions through radiation and cloud feedback, based on the diagnosed mass mixing ratios of bulk aerosols. The base simulation shows that BCC-GEOS-Chem v2.0 with full aerosol–cloud–radiation interactions reproduce the global spatial distributions of radiation and cloud properties from satellite observations and reanalysis dataset. Sensitivity experiments indicate that the model is able to simulate the impact of aerosols on radiative budget, e.g., decreasing SWDOWN, OLR, and LWCRF, and increasing SWCRF. Further analyses by separating the role of ARIs and ACIs indicate that ACIs promote cloud development but suppress precipitation for the global average, while the contributions from ARIs are rather small.

BCC-GEOS-Chem v2.0 can now perform at a high resolution at T159L72 (0.75° × 0.75° and 72 vertical layers with a top at 0.01 hPa), taking the advantages of the BCC-GC-HEMCO interface that enables seamless integration of the GEOS-Chem chemical module with ESMs across customizable grid configurations. Compared with the T42L26 simulation, the high-resolution simulation much better resolves the fine-scale plume transport dynamics, and also significantly improve the ability to capture the pollution hotspot of NO_2 and $PM_{2.5}$ as well as the low ozone concentration in high-NO_x environment in wintertime China. The shows attractive potential for future applications in air quality simulation.

In summary, the development of the BCC-GEOS-Chem v2.0 model provides a useful framework for investigating climate–chemistry interactions and for future projections of global atmospheric chemistry. Its high-resolution configuration can also be applied to air quality forecasts. Nevertheless, there are still limitations in this model that should be addressed in future development. First, although the UCX interactive stratospheric chemistry scheme has been implemented, biases remain in the simulation of stratospheric ozone and will require further improvement. The feedbacks through methane-OH interactions are not fully represented in the current model configuration and should be addressed by introducing unbiased methane sources. In addition, the implementation of size-resolved aerosol schemes will be a priority moving forward, as they will enable a more accurate representation of aerosol feedbacks. Furthermore, the enormous amount of time and computational resources for T159L72 high-resolution is still a major obstacle. We are planning to improve this high-resolution version of BCC-GEOS-Chem v2.0 with enhanced computational efficiency in our next-phase implementation, enabling its broader application in the research of global climate change and atmospheric chemistry.

Code availability. The GEOS-Chem model is maintained at the Harvard Atmospheric Chemistry Modelling group, which can be obtained at https://doi.org/10.5281/zenodo.7271960 (last access: 1 April 2025). The HEMCO modules used in this paper is permanently archived at https://zenodo.org/records/18862941 (Sun, 2026b). The BCC-GEOS-Chem v2.0 code can be accessed at a DOI repository https://zenodo.org/records/18448688 (Sun, 2026a), and model outputs for 2012–2014 are available at https://zenodo.org/records/16734757 (Sun, 2025). All source code and data can also be accessed by contacting the corresponding authors Lin Zhang (zhanglg@pku.edu.cn).

Author contributions. LZ designed and led the project. RZS and XL developed the model source code with substantial contributions from HPL, WTW, JZ, and FZ. RZS performed model simulations, analysed data, and prepared the figures with contributions from XPY, LJY, and, HLW. RZS, XL, and LZ wrote the paper. All authors contributed to the interpretation of results and improvement of the paper.

Competing interests. The authors declare that they have no conflict of interest.

Acknowledgements. This research was supported by the National Key Research and Development Program of China (2023YFC3706104) and the National Natural Science Foundation of China (grant no. 42275106 and no. 42522505). This research is also supported by the Guangdong Basic and Applied Basic Research Foundation (2025B1515020034). We thank the GEOS-Chem support team for facilitating the open-source development of GEOS–Chem model.

Financial support. This research was supported by the National Key Research and Development Program of China (2023YFC3706104) and the National Natural Science Foundation of China (grant no. 42275106 and no. 42522505). This research is also supported by the Guangdong Basic and Applied Basic Research Foundation (2025B1515020034).

References

Abel, D., Holloway, T., Kladar, R. M., Meier, P., Ahl, D., Harkey, M., and Patz, J.: Response of Power Plant Emissions to Ambient Temperature in the Eastern United States, Environ. Sci. Technol., 51, 5838–5846, https://doi.org/10.1021/acs.est.6b06201, 2017.

Alizadeh-Choobari, O. and Gharaylou, M.: Aerosol impacts on radiative and microphysical properties of clouds and precipitation formation, Atmospheric Research, 185, 53–64, https://doi.org/10.1016/j.atmosres.2016.10.021, 2017.

Global Fire Emissions Database, Version 4.1 (GFEDv4), https://doi.org/10.3334/ORNLDAAC/1293: https://daac.ornl.gov/cgi-bin/dsviewer.pl?ds_id=1293, last access: 3 May 2025.

Local Versus Nonlocal Boundary-Layer Diffusion in a Global Climate Model in: Journal of Climate Volume 6 Issue 10 (1993): https://journals.ametsoc.org/view/journals/clim/6/10/1520-0442_1993_006_1825_lvnbld_2_0_co_2.xml, last access: 1 January 2025.

The Role of Stratospheric Ozone in the Zonal and Seasonal Radiative Energy Balance of the Earth-Troposphere System in: Journal of the Atmospheric Sciences Volume 36 Issue 6 (1979): https://journals.ametsoc.org/view/journals/atsc/36/6/1520-0469_1979_036_1084_trosoi_2_0_co_2.xml, last access: 24 May 2025.

Two-Dimensional Semi-Lagrangian Transport with Shape-Preserving Interpolation in: Monthly Weather Review Volume 117 Issue 1 (1989): https://journals.ametsoc.org/view/journals/mwre/117/1/1520-0493_1989_117_0102_tdsltw_2_0_co_2.xml, last access: 24 May 2025.

Bates, K. H., Jacob, D. J., Li, K., Ivatt, P. D., Evans, M. J., Yan, Y., and Lin, J.: Development and evaluation of a new compact mechanism for aromatic oxidation in atmospheric models, Atmospheric Chemistry and Physics, 21, 18351–18374, https://doi.org/10.5194/acp-21-18351-2021, 2021.

Bey, I., Jacob, D. J., Yantosca, R. M., Logan, J. A., Field, B. D., Fiore, A. M., Li, Q., Liu, H. Y., Mickley, L. J., and Schultz, M. G.: Global modeling of tropospheric chemistry with assimilated meteorology: Model description and evaluation, J. Geophys. Res., 106, 23073–23095, https://doi.org/10.1029/2001JD000807, 2001.

Boucher, O. and Lohmann, U.: The sulfate-CCN-cloud albedo effect., Tellus B, 47, 281–300, https://doi.org/10.1034/j.1600-0889.47.issue3.1.x, 1995.

Briegleb, B. P.: Delta‐Eddington approximation for solar radiation in the NCAR community climate model, J. Geophys. Re s., 97, 7603–7612, https://doi.org/10.1029/92JD00291, 1992.

Chapman, E. G., Jr, W. I. G., Easter, R. C., Barnard, J. C., Ghan, S. J., Pekour, M. S., and Fast, J. D.: Coupling aerosol-cloud -radiative processes in the WRF-Chem model: Investigating the radiative impact of elevated point sources, Atmos. Che m. Phys., 2009.

Collins, W. D.: A global signature of enhanced shortwave absorption by clouds, J. Geophys. Res., 103, 31669–31679, https:/ /doi.org/10.1029/1998JD200022, 1998.

Collins, W. D., Hackney, J. K., and Edwards, D. P.: An updated parameterization for infrared emission and absorption by wa ter vapor in the National Center for Atmospheric Research Community Atmosphere Model, J.‐Geophys.‐Res., 107, h ttps://doi.org/10.1029/2001JD001365, 2002.

Collins, W. D., Rasch, P. J., Boville, B. A., Hack, J. J., McCaa, J. R., Williamson, D. L., Kiehl, J. T., Briegleb, B., Bitz, C., L in, S.-J., Zhang, M., and Dai, Y.: Description of the NCAR Community Atmosphere Model (CAM 3.0), n.d.

Collins, W. J., Lamarque, J.-F., Schulz, M., Boucher, O., Eyring, V., Hegglin, I., Maycock, A., Myhre, G., Prather, M., Shin dell, D., and Smith, S. J.: AerChemMIP: quantifying the effects of chemistry and aerosols in CMIP6, Geosci. Model De v., 2017.

Cooper, O. R., Parrish, D. D., Ziemke, J., Balashov, N. V., Cupeiro, M., Galbally, I. E., Gilge, S., Horowitz, L., Jensen, N. R., Lamarque, J.-F., Naik, V., Oltmans, S. J., Schwab, J., Shindell, D. T., Thompson, A. M., Thouret, V., Wang, Y., and Zbinden, R. M.: Global distribution and trends of tropospheric ozone: An observation-based review, Elementa: Science of the Anthropocene, 2, 000029, https://doi.org/10.12952/journal.elementa.000029, 2014.

Craig, A. P., Vertenstein, M., and Jacob, R.: A new flexible coupler for earth system modeling developed for CCSM4 and C ESM1, The International Journal of High Performance Computing Applications, 26, 31–42, https://doi.org/10.1177/109 4342011428141, 2012.

Damian, V., Sandu, A., Damian, M., Potra, F., and Carmichael, G. R.: The kinetic preprocessor KPP-a software environment for solving chemical kinetics, Computers & Chemical Engineering, 26, 1567–1579, https://doi.org/10.1016/S0098-135 4(02)00128-X, 2002.

De Smedt, I., Stavrakou, T., Hendrick, F., Danckaert, T., Vlemmix, T., Pinardi, G., Theys, N., Lerot, C., Gielen, C., Vigouro ux, C., Hermans, C., Fayt, C., Veefkind, P., Müller, J.-F., and Van Roozendael, M.: Diurnal, seasonal and long-term var iations of global formaldehyde columns inferred from combined OMI and GOME-2 observations, Atmospheric Chemis try and Physics, 15, 12519–12545, https://doi.org/10.5194/acp-15-12519-2015, 2015.

Deeter, M. N.: Impacts of MOPITT cloud detection revisions on observation frequency and mapping of highly polluted scenes, Remote Sensing of Environment, 2021.

Duncan Fairlie, T., Jacob, D. J., and Park, R. J.: The impact of transpacific transport of mineral dust in the United States, Atmospheric Environment, 41, 1251–1266, https://doi.org/10.1016/j.atmosenv.2006.09.048, 2007.

Eastham, S. D. and Jacob, D. J.: Limits on the ability of global Eulerian models to resolve intercontinental transport of chemical plumes, Atmospheric Chemistry and Physics, 17, 2543–2553, https://doi.org/10.5194/acp-17-2543-2017, 2017.

Eastham, S. D., Weisenstein, D. K., and Barrett, S. R. H.: Development and evaluation of the unified tropospheric–stratospheric chemistry extension (UCX) for the global chemistry-transport model GEOS-Chem, Atmospheric Environment, 89, 52–63, https://doi.org/10.1016/j.atmosenv.2014.02.001, 2014.

Eastham, S. D., Long, M. S., Keller, C. A., Lundgren, E., Yantosca, R. M., Zhuang, J., Li, C., Lee, C. J., Yannetti, M., Auer, B. M., Clune, T. L., Kouatchou, J., Putman, W. M., Thompson, M. A., Trayanov, A. L., Molod, A. M., Martin, R. V., and Jacob, D. J.: GEOS-Chem High Performance (GCHP v11-02c): a next-generation implementation of the GEOS-Chem chemical transport model for massively parallel applications, Geosci. Model Dev., 2018.

Emmons, L. K., Deeter, M. N., Gille, J. C., Edwards, D. P., Attié, J.‐L., Warner, J., Ziskin, D., Francis, G., Khattatov, B., Yudin, V., Lamarque, J.‐F., Ho, S.‐P., Mao, D., Chen, J. S., Drummond, J., Novelli, P., Sachse, G., Coffey, M. T., Hannigan, J. W., Gerbig, C., Kawakami, S., Kondo, Y., Takegawa, N., Schlager, H., Baehr, J., and Ziereis, H.: Validation of Measurements of Pollution in the Troposphere (MOPITT) CO retrievals with aircraft in situ profiles, J. Geophys. Res., 109, 2003JD004101, https://doi.org/10.1029/2003JD004101, 2004.

Fan, J., Wang, Y., Rosenfeld, D., and Liu, X.: Review of Aerosol–Cloud Interactions: Mechanisms, Significance, and Challenges, Journal of the Atmospheric Sciences, 73, 4221–4252, https://doi.org/10.1175/JAS-D-16-0037.1, 2016.

Feng, J., Zhao, C., Du, Q., Yang, Z., and Jin, C.: Amending the algorithm of aerosol–radiation interactions in WRF-Chem (v4.4), Geosci. Model Dev., 18, 585–603, https://doi.org/10.5194/gmd-18-585-2025, 2025.

Feng, X., Lin, H., Fu, T.-M., Sulprizio, M. P., Zhuang, J., Jacob, D. J., Tian, H., Ma, Y., Zhang, L., Wang, X., Chen, Q., and Han, Z.: WRF-GC (v2.0): online two-way coupling of WRF (v3.9.1.1) and GEOS-Chem (v12.7.2) for modeling regional atmospheric chemistry–meteorology interactions, Geoscientific Model Development, 14, 3741–3768, https://doi.org/10.5194/gmd-14-3741-2021, 2021.

Fiore, A. M., Naik, V., Spracklen, D. V., Steiner, A., Unger, N., Prather, M., Bergmann, D., Cameron-Smith, P. J., Cionni, I., Collins, W. J., Dalsøren, S., Eyring, V., Folberth, G. A., Ginoux, P., Horowitz, L. W., Josse, B., Lamarque, J.-F., MacKenzie, I. A., Nagashima, T., O'Connor, F. M., Righi, M., Rumbold, S. T., Shindell, D. T., Skeie, R. B., Sudo, K., Szopa, S., Takemura, T., and Zeng, G.: Global air quality and climate, Chem. Soc. Rev., 41, 6663, https://doi.org/10.1039/c2cs35095e, 2012.

Fountoukis, C. and Nenes, A.: ISORROPIA II: a computationally efficient thermodynamic equilibrium model for K+–Ca2+–Mg2+–NH4+–Na+–SO42−–NO3−–Cl−–H2O aerosols, Atmospheric Chemistry and Physics, 7, 4639–4659, https://doi.org/10.5194/acp-7-4639-2007, 2007.

Fritz, T. M., Eastham, S. D., Emmons, L. K., Lin, H., Lundgren, E. W., Goldhaber, S., Barrett, S. R. H., and Jacob, D. J.: Implementation and evaluation of the GEOS-Chem chemistry module version 13.1.2 within the Community Earth System Model v2.1, Geoscientific Model Development, 15, 8669–8704, https://doi.org/10.5194/gmd-15-8669-2022, 2022.

Gao, Y., Kou, W., Cheng, W., Guo, X., Qu, B., Wu, Y., Zhang, S., Liao, H., Chen, D., Leung, L. R., Wild, O., Zhang, J., Lin, G., Su, H., Cheng, Y., Pöschl, U., Pozzer, A., Zhang, L., Lamarque, J., Guenther, A. B., Brasseur, G., Liu, Z., Lu, H., Li, C., Zhao, B., Wang, S., Huang, X., Pan, J., Liu, G., Liu, X., Lin, H., Zhao, Y., Zhao, C., Meng, J., Yao, X., Gao, H., and Wu, L.: Reducing Long‐Standing Surface Ozone Overestimation in Earth System Modeling by High‐Resolution Simulation and Dry Deposition Improvement, J Adv Model Earth Syst, 17, e2023MS004192, https://doi.org/10.1029/2023MS004192, 2025.

Gong, S. L.: A parameterization of sea‐salt aerosol source function for sub‐ and super‐micron particles, Global Biogeochemical Cycles, 17, 2003GB002079, https://doi.org/10.1029/2003GB002079, 2003.

Guenther, A. B., Jiang, X., Heald, C. L., Sakulyanontvittaya, T., Duhl, T., Emmons, L. K., and Wang, X.: The Model of Emissions of Gases and Aerosols from Nature version 2.1 (MEGAN2.1): an extended and updated framework for modeling biogenic emissions, Geoscientific Model Development, 5, 1471–1492, https://doi.org/10.5194/gmd-5-1471-2012, 2012.

Haywood, J. and Boucher, O.: Estimates of the direct and indirect radiative forcing due to tropospheric aerosols: A review, Reviews of Geophysics, 38, 513–543, https://doi.org/10.1029/1999RG000078, 2000.

Hess, M., Koepke, P., and Schult, I.: Optical Properties of Aerosols and Clouds: The Software Package OPAC, Bull. Amer. Meteor. Soc., 79, 831–844, https://doi.org/10.1175/1520-0477(1998)079<0831:OPOAAC>2.0.CO;2, 1998.

Horowitz, L. W., Walters, S., Mauzerall, D. L., Emmons, L. K., Rasch, P. J., Granier, C., Tie, X., Lamarque, J., Schultz, M. G., Tyndall, G. S., Orlando, J. J., and Brasseur, G. P.: A global simulation of tropospheric ozone and related tracers: Description and evaluation of MOZART, version 2, J. Geophys. Res., 108, https://doi.org/10.1029/2002jd002853, 2003.

Hu, L., Jacob, D. J., Liu, X., Zhang, Y., Zhang, L., Kim, P. S., Sulprizio, M. P., and Yantosca, R. M.: Global budget of tropospheric ozone: Evaluating recent model advances with satellite (OMI), aircraft (IAGOS), and ozonesonde observations, Atmospheric Environment, 167, 323–334, https://doi.org/10.1016/j.atmosenv.2017.08.036, 2017.

Hu, L., Keller, C. A., Long, M. S., Sherwen, T., Auer, B., Da Silva, A., Nielsen, J. E., Pawson, S., Thompson, M. A., Trayanov, A. L., Travis, K. R., Grange, S. K., Evans, M. J., and Jacob, D. J.: Global simulation of tropospheric chemistry at 12.5 km resolution: performance and evaluation of the GEOS-Chem chemical module (v10-1) within the NASA GEOS Earth system model (GEOS-5 ESM), Geosci. Model Dev., 11, 4603–4620, https://doi.org/10.5194/gmd-11-4603-2018, 2018.

Huang, G., Liu, X., Chance, K., Yang, K., Bhartia, P. K., Cai, Z., Allaart, M., Ancellet, G., Calpini, B., Coetzee, G. J. R., Cuevas-Agulló, E., Cupeiro, M., De Backer, H., Dubey, M. K., Fuelberg, H. E., Fujiwara, M., Godin-Beekmann, S., Hall, T. J., Johnson, B., Joseph, E., Kivi, R., Kois, B., Komala, N., König-Langlo, G., Laneve, G., Leblanc, T., Marchand, M., Minschwaner, K. R., Morris, G., Newchurch, M. J., Ogino, S.-Y., Ohkawara, N., Piters, A. J. M., Posny, F., Querel, R., Scheele, R., Schmidlin, F. J., Schnell, R. C., Schrems, O., Selkirk, H., Shiotani, M., Skrivánková, P., Stübi, R., Taha, G., Tarasick, D. W., Thompson, A. M., Thouret, V., Tully, M. B., Van Malderen, R., Vömel, H., Von Der Gathen, P., Witte, J. C., and Yela, M.: Validation of 10-year SAO OMI Ozone Profile (PROFOZ) product using ozonesonde observations, Atmos. Meas. Tech., 10, 2455–2475, https://doi.org/10.5194/amt-10-2455-2017, 2017.

Huang, G., Liu, X., Chance, K., Yang, K., and Cai, Z.: Validation of 10-year SAO OMI ozone profile (PROFOZ) product using Aura MLS measurements, Atmospheric Measurement Techniques, 11, 17–32, https://doi.org/10.5194/amt-11-17-2018, 2018.

Hudman, R. C., Moore, N. E., Mebust, A. K., Martin, R. V., Russell, A. R., Valin, L. C., and Cohen, R. C.: Steps towards a mechanistic model of global soil nitric oxide emissions: implementation and space based-constraints, Atmospheric Chemistry and Physics, 12, 7779–7795, https://doi.org/10.5194/acp-12-7779-2012, 2012.

Huffman, G. J., Adler, R. F., Morrissey, M. M., Bolvin, D. T., Curtis, S., Joyce, R., McGavock, B., and Susskind, J.: Global Precipitation at One-Degree Daily Resolution from Multisatellite Observations, J. Hydrometeor, 2, 36–50, https://doi.org/10.1175/1525-7541(2001)002<0036:GPAODD>2.0.CO;2, 2001.

Isaksen, I. S. A., Granier, C., Myhre, G., Berntsen, T. K., Dalsøren, S. B., Gauss, M., Klimont, Z., Benestad, R., Bousquet, P., Collins, W., Cox, T., Eyring, V., Fowler, D., Fuzzi, S., Jöckel, P., Laj, P., Lohmann, U., Maione, M., Monks, P., Prevot, A. S. H., Raes, F., Richter, A., Rognerud, B., Schulz, M., Shindell, D., Stevenson, D. S., Storelvmo, T., Wang, W.-C., Van Weele, M., Wild, M., and Wuebbles, D.: Atmospheric composition change: Climate–Chemistry interactions, Atmospheric Environment, 43, 5138–5192, https://doi.org/10.1016/j.atmosenv.2009.08.003, 2009.

IPCC: Climate Change 2013: The Physical Science Basis. Contribution of Working Group I to the Fifth Assessment Report of the Intergovernmental Panel on Climate Change, edited by: Stocker, T. F., Qin, D., Plattner, G.-K., Tignor, M., Allen, S. K., Boschung, J., Nauels, A., Xia, Y., Bex, V., and Midgley, P. M., Cambridge University Press, Cambridge, United Kingdom and New York, NY, USA, 1535 pp., https://doi.org/10.1017/CBO9781107415324, 2013.

IPCC: Climate Change 2021: The Physical Science Basis. Contribution of Working Group I to the Sixth Assessment Report of the Intergovernmental Panel on Climate Change, [Masson-Delmotte, V., P. Zhai, A. Pirani, S.L. Connors, C. Péan, S. Berger, N. Caud, Y. Chen, L. Goldfarb, M.I. Gomis, M. Huang, K. Leitzell, E. Lonnoy, J.B.R. Matthews, T.K. Maycock, T. Waterfield, O. Yelekçi, R. Yu, and B. Zhou (eds.)]. Cambridge University Press, Cambridge, United Kingdom and New York, NY, USA, In press, doi:10.1017/9781009157896.

Jacob, D. J. and Winner, D. A.: Effect of climate change on air quality, Atmospheric Environment, 43, 51–63, https://doi.org/10.1016/j.atmosenv.2008.09.051, 2009.

Jaeglé, L., Quinn, P. K., Bates, T. S., Alexander, B., and Lin, J.-T.: Global distribution of sea salt aerosols: new constraints from in situ and remote sensing observations, Atmospheric Chemistry and Physics, 11, 3137–3157, https://doi.org/10.5194/acp-11-3137-2011, 2011.

John, J. G., Fiore, A. M., Naik, V., Horowitz, L. W., and Dunne, J. P.: Climate versus emission drivers of methane lifetime against loss by tropospheric OH from 1860–2100, Atmospheric Chemistry and Physics, 12, 12021–12036, https://doi.org/10.5194/acp-12-12021-2012, 2012.

Jones, C. D., Arora, V., Friedlingstein, P., Bopp, L., Brovkin, V., Dunne, J., Graven, H., Hoffman, F., Ilyina, T., John, J. G., Jung, M., Kawamiya, M., Koven, C., Pongratz, J., Raddatz, T., Randerson, J. T., and Zaehle, S.: C4MIP – The Coupled Climate–Carbon Cycle Model Intercomparison Project: experimental protocol for CMIP6, Geosci. Model Dev., 2016.

Kato, S., Rose, F. G., Rutan, D. A., Thorsen, T. J., Loeb, N. G., Doelling, D. R., Huang, X., Smith, W. L., Su, W., and Ham, S.-H.: Surface Irradiances of Edition 4.0 Clouds and the Earth’s Radiant Energy System (CERES) Energy Balanced and Filled (EBAF) Data Product, Journal of Climate, 31, 4501–4527, https://doi.org/10.1175/JCLI-D-17-0523.1, 2018.

Keller, C. A., Long, M. S., Yantosca, R. M., Da Silva, A. M., Pawson, S., and Jacob, D. J.: HEMCO v1.0: a versatile, ESMF-compliant component for calculating emissions in atmospheric models, Geosci. Model Dev., 7, 1409–1417, https://doi.org/10.5194/gmd-7-1409-2014, 2014.

Kiehl, J. T. and Briegleb, B. P.: A new parameterization of the absorptance due to the 15‐μm band system of carbon dioxide, J. Geophys. Res., 96, 9013–9019, https://doi.org/10.1029/89JD00993, 1991.

Kodros, J. K. and Pierce, J. R.: Important global and regional differences in aerosol cloud‐albedo effect estimates between simulations with and without prognostic aerosol microphysics, JGR Atmospheres, 122, 4003–4018, https://doi.org/10.1002/2016JD025886, 2017.

Lamsal, L. N., Krotkov, N. A., Vasilkov, A., Marchenko, S., Qin, W., Yang, E.-S., Fasnacht, Z., Joiner, J., Choi, S., Haffner, D., Swartz, W. H., Fisher, B., and Bucsela, E.: Ozone Monitoring Instrument (OMI) Aura nitrogen dioxide standard product version 4.0 with improved surface and cloud treatments, Atmos. Meas. Tech., 14, 455–479, https://doi.org/10.5194/amt-14-455-2021, 2021.

Li, W., Zhang, Y., Shi, X., Zhou, W., Huang, A., Mu, M., Qiu, B., and Ji, J.: Development of Land Surface Model BCC_AVIM2.0 and Its Preliminary Performance in LS3MIP/CMIP6, Journal of Meteorological Research, 33, 2019.

Lin, H., Feng, X., Fu, T.-M., Tian, H., Ma, Y., Zhang, L., Jacob, D. J., Yantosca, R. M., Sulprizio, M. P., Lundgren, E. W., Zhuang, J., Zhang, Q., Lu, X., Zhang, L., Shen, L., Guo, J., Eastham, S. D., and Keller, C. A.: WRF-GC (v1.0): online coupling of WRF (v3.9.1.1) and GEOS-Chem (v12.2.1) for regional atmospheric chemistry modeling – Part 1: Description of the one-way model, Geoscientific Model Development, 13, 3241–3265, https://doi.org/10.5194/gmd-13-3241-2020, 2020.

Lin, H., Jacob, D. J., Lundgren, E. W., Sulprizio, M. P., Keller, C. A., Fritz, T. M., Eastham, S. D., Emmons, L. K., Campbell, P. C., Baker, B., Saylor, R. D., and Montuoro, R.: Harmonized Emissions Component (HEMCO) 3.0 as a versatile emissions component for atmospheric models: application in the GEOS-Chem, NASA GEOS, WRF-GC, CESM2, NOAA GEFS-Aerosol, and NOAA UFS models, Geoscientific Model Development, 14, 5487–5506, https://doi.org/10.5194/gmd-14-5487-2021, 2021.

Lin, H., Long, M. S., Sander, R., Sandu, A., Yantosca, R. M., Estrada, L. A., Shen, L., and Jacob, D. J.: An Adaptive Auto‐Reduction Solver for Speeding Up Integration of Chemical Kinetics in Atmospheric Chemistry Models: Implementatio n and Evaluation in the Kinetic Pre‐Processor (KPP) Version 3.0.0, J Adv Model Earth Syst, 15, e2022MS003293, https://doi.org/10.1029/2022MS003293, 2023.

Lin, H., Emmons, L. K., Lundgren, E. W., Yang, L. H., Feng, X., Dang, R., Zhai, S., Tang, Y., Kelp, M. M., Colombi, N. K., Eastham, S. D., Fritz, T. M., and Jacob, D. J.: Intercomparison of GEOS-Chem and CAM-chem tropospheric oxidant chemistry within the Community Earth System Model version 2 (CESM2), Atmos. Chem. Phys., 24, 8607–8624, https://doi.org/10.5194/acp-24-8607-2024, 2024.

Liu, H., Jacob, D. J., Bey, I., and Yantosca, R. M.: Constraints from210 Pb and7 Be on wet deposition and transport in a global three‐dimensional chemical tracer model driven by assimilated meteorological fields, J. Geophys. Res., 106, 12109–12128, https://doi.org/10.1029/2000JD900839, 2001.

Liu, X., Bhartia, P. K., Chance, K., Spurr, R. J. D., and Kurosu, T. P.: Ozone profile retrievals from the Ozone Monitoring Instrument, Atmospheric Chemistry and Physics, 10, 2521–2537, https://doi.org/10.5194/acp-10-2521-2010, 2010.

Lohmann, U. and Feichter, J.: Global indirect aerosol effects: a review, Atmos. Chem. Phys., 2005.

Long, M. S., Yantosca, R., Nielsen, J. E., Keller, C. A., Da Silva, A., Sulprizio, M. P., Pawson, S., and Jacob, D. J.: Development of a grid-independent GEOS-Chem chemical transport model (v9-02) as an atmospheric chemistry module for Earth system models, Geosci. Model Dev., 8, 595–602, https://doi.org/10.5194/gmd-8-595-2015, 2015.

Lu, X., Zhang, L., and Shen, L.: Meteorology and Climate Influences on Tropospheric Ozone: a Review of Natural Sources, Chemistry, and Transport Patterns, Curr Pollution Rep, 5, 238–260, https://doi.org/10.1007/s40726-019-00118-3, 2019.

Lu, X., Zhang, L., Wu, T., Long, M. S., Wang, J., Jacob, D. J., Zhang, F., Zhang, J., Eastham, S. D., Hu, L., Zhu, L., Liu, X., and Wei, M.: Development of the global atmospheric chemistry general circulation model BCC-GEOS-Chem v1.0: model description and evaluation, Geoscientific Model Development, 13, 3817–3838, https://doi.org/10.5194/gmd-13-3817-2020, 2020.

Lu, X., Jacob, D. J., Zhang, Y., Maasakkers, J. D., Sulprizio, M. P., Shen, L., Qu, Z., Scarpelli, T. R., Nesser, H., Yantosca, R. M., Sheng, J., Andrews, A., Parker, R. J., Boesch, H., Bloom, A. A., and Ma, S.: Global methane budget and trend, 2010–2017: complementarity of inverse analyses using in situ (GLOBALVIEWplus CH4 ObsPack) and satellite (GOSAT) observations, Atmospheric Chemistry and Physics, 21, 4637–4657, https://doi.org/10.5194/acp-21-4637-2021, 2021.

Lu, X., Liu, Y., Su, J., Weng, X., Ansari, T., Zhang, Y., He, G., Zhu, Y., Wang, H., Zeng, G., Li, J., He, C., Li, S., Amnuaylojaroen, T., Butler, T., Fan, Q., Fan, S., Forster, G. L., Gao, M., Hu, J., Kanaya, Y., Latif, M. T., Lu, K., Nédélec, P., Nowack, P., Sauvage, B., Xu, X., Zhang, L., Li, K., Koo, J.-H., and Nagashima, T.: Tropospheric ozone trends and attributions over East and Southeast Asia in 1995–2019: An integrated assessment using statistical methods, machine learning models, and multiple chemical transport models, https://doi.org/10.5194/egusphere-2024-3702, 17 December 2024.

McDuffie, E. E., Smith, S. J., O'Rourke, P., Tibrewal, K., Venkataraman, C., Marais, E. A., Zheng, B., Crippa, M., Brauer, M., and Martin, R. V.: A global anthropogenic emission inventory of atmospheric pollutants from sector- and fuel-specific sources (1970–2017): an application of the Community Emissions Data System (CEDS), Earth Syst. Sci. Data, 12, 3413–3442, https://doi.org/10.5194/essd-12-3413-2020, 2020.

McLinden, C. A., Olsen, S. C., Hannegan, B., Wild, O., Prather, M. J., and Sundet, J.: Stratospheric ozone in 3-D models: A simple chemistry and the cross-tropopause flux, J. Geophys. Res., 105, 14653–14665, https://doi.org/10.1029/2000jd900124, 2000.

Naik, V., Voulgarakis, A., Fiore, A. M., Horowitz, L. W., Lamarque, J.-F., Lin, M., Prather, M. J., Young, P. J., Bergmann, D., Cameron-Smith, P. J., Cionni, I., Collins, W. J., Dalsøren, S. B., Doherty, R., Eyring, V., Faluvegi, G., Folberth, G. A., Josse, B., Lee, Y. H., MacKenzie, I. A., Nagashima, T., van Noije, T. P. C., Plummer, D. A., Righi, M., Rumbold, S. T., Skeie, R., Shindell, D. T., Stevenson, D. S., Strode, S., Sudo, K., Szopa, S., and Zeng, G.: Preindustrial to present-day changes in tropospheric hydroxyl radical and methane lifetime from the Atmospheric Chemistry and Climate Model Intercomparison Project (ACCMIP), Atmospheric Chemistry and Physics, 13, 5277–5298, https://doi.org/10.5194/acp-13-5277-2013, 2013.

Nicely, J. M., Duncan, B. N., Hanisco, T. F., Wolfe, G. M., Salawitch, R. J., Deushi, M., Haslerud, A. S., Jöckel, P., Josse, B., Kinnison, D. E., Klekociuk, A., Manyin, M. E., Marécal, V., Morgenstern, O., Murray, L. T., Myhre, G., Oman, L. D., Pitari, G., Pozzer, A., Quaglia, I., Revell, L. E., Rozanov, E., Stenke, A., Stone, K., Strahan, S., Tilmes, S., Tost, H., Westervelt, D. M., and Zeng, G.: A machine learning examination of hydroxyl radical differences among model simulations for CCMI-1, Atmos. Chem. Phys., 20, 1341–1361, https://doi.org/10.5194/acp-20-1341-2020, 2020.

Olson, D. M., Dinerstein, E., Wikramanayake, E. D., Burgess, N. D., Powell, G. V. N., Underwood, E. C., D'Amico, J. A., Itoua, I., Strand, H. E., Morrison, J. C., Loucks, J., Allnutt, T. F., Ricketts, T. H., Kura, Y., Lamoreux, J. F., Hedao, P., and Kassem, K. R.: Terrestrial Ecoregions of the World: A New Map of Life on Earth, n.d.

Pendharkar, J., Figueroa, S. N., Vara-Vela, A., Krishna, R. P. M., Schuch, D., Kubota, P. Y., Alvim, D. S., Vendrasco, E. P., Gomes, H. B., Nobre, P., and Herdies, D. L.: Towards Unified Online-Coupled Aerosol Parameterization for the Brazilian Global Atmospheric Model (BAM): Aerosol–Cloud Microphysical–Radiation Interactions, 2023.

Peng, Y. and Lohmann, U.: Sensitivity study of the spectral dispersion of the cloud droplet size distribution on the indirect aerosol effect, Geophysical Research Letters, 30, 2003GL017192, https://doi.org/10.1029/2003GL017192, 2003.

Pfister, G., Hess, P. G., Emmons, L. K., Lamarque, J.-F., Wiedinmyer, C., Edwards, D. P., Pétron, G., Gille, J. C., and Sachse, G. W.: Quantifying CO emissions from the 2004 Alaskan wildfires using MOPITT CO data, Geophysical Research Letters, 32, 2005GL022995, https://doi.org/10.1029/2005GL022995, 2005.

Pound, R. J., Sherwen, T., Helmig, D., Carpenter, L. J., and Evans, M. J.: Influences of oceanic ozone deposition on tropospheric photochemistry, Atmos. Chem. Phys., 20, 4227–4239, https://doi.org/10.5194/acp-20-4227-2020, 2020.

Price, C. and Rind, D.: A simple lightning parameterization for calculating global lightning distributions, Journal of Geophysical Research: Atmospheres, 97, 9919–9933, https://doi.org/10.1029/92JD00719, 1992.

Quaas, J., Boucher, O., and Lohmann, U.: Constraining the total aerosol indirect effect in the LMDZ and ECHAM4 GCMs using MODIS satellite data, Atmos. Chem. Phys., 2006.

Ramanathan, V. and Downey, P.: A nonisothermal emissivity and absorptivity formulation for water vapor, J. Geophys. Res., 91, 8649–8666, https://doi.org/10.1029/JD091iD08p08649, 1986.

Reddington, C. L., Carslaw, K. S., Stier, P., Schutgens, N., Coe, H., Liu, D., Allan, J., Browse, J., Pringle, K. J., Lee, L. A., Yoshioka, M., Johnson, J. S., Regayre, L. A., Spracklen, D. V., Mann, G. W., Clarke, A., Hermann, M., Henning, S., Wex, H., Kristensen, T. B., Leaitch, W. R., Pöschl, U., Rose, D., Andreae, M. O., Schmale, J., Kondo, Y., Oshima, N., Schwarz, J. P., Nenes, A., Anderson, B., Roberts, G. C., Snider, J. R., Leck, C., Quinn, P. K., Chi, X., Ding, A., Jimenez, J. L., and Zhang, Q.: The Global Aerosol Synthesis and Science Project (GASSP): Measurements and Modeling to Reduce Uncertainty, Bulletin of the American Meteorological Society, 98, 1857–1877, https://doi.org/10.1175/BAMS-D-15-00317.1, 2017.

Rosenfeld, D., Lohmann, U., Raga, G. B., O'Dowd, C. D., Kulmala, M., Fuzzi, S., Reissell, A., and Andreae, M. O.: Flood or Drought: How Do Aerosols Affect Precipitation?, Science, 321, 1309–1313, https://doi.org/10.1126/science.1160606, 2008.

Saunois, M., Martinez, A., Poulter, B., Zhang, Z., Raymond, P., Regnier, P., Canadell, J. G., Jackson, R. B., Patra, P. K., Bousquet, P., Ciais, P., Dlugokencky, E. J., Lan, X., Allen, G. H., Bastviken, D., Beerling, D. J., Belikov, D. A., Blake, D. R., Castaldi, S., Crippa, M., Deemer, B. R., Dennison, F., Etiope, G., Gedney, N., Höglund-Isaksson, L., Holgerson, M. A., Hopcroft, P. O., Hugelius, G., Ito, A., Jain, A. K., Janardanan, R., Johnson, M. S., Kleinen, T., Krummel, P., Lauerwald, R., Li, T., Liu, X., McDonald, K. C., Melton, J. R., Mühle, J., Müller, J., Murguia-Flores, F., Niwa, Y., Noce, S., Pan, S., Parker, R. J., Peng, C., Ramonet, M., Riley, W. J., Rocher-Ros, G., Rosentreter, J. A., Sasakawa, M., Segers, A., Smith, S. J., Stanley, E. H., Thanwerdas, J., Tian, H., Tsuruta, A., Tubiello, F. N., Weber, T. S., Van Der Werf, G., Worthy, D. E., Xi, Y., Yoshida, Y., Zhang, W., Zheng, B., Zhu, Q., Zhu, Q., and Zhuang, Q.: Global Methane Budget 2000–2020, https://doi.org/10.5194/essd-2024-115, 6 June 2024.

Sauvage, B., Martin, R. V., Van Donkelaar, A., and Ziemke, J. R.: Quantification of the factors controlling tropical tropospheric ozone and the South Atlantic maximum, J. Geophys. Res., 112, 2006JD008008, https://doi.org/10.1029/2006JD008008, 2007.

Schwantes, R. H., Lacey, F. G., Tilmes, S., Emmons, L. K., Lauritzen, P. H., Walters, S., Callaghan, P., Zarzycki, C. M., Barth, M. C., Jo, D. S., Bacmeister, J. T., Neale, R. B., Vitt, F., Kluzek, E., Roozitalab, B., Hall, S. R., Ullmann, K., Warneke, C., Peischl, J., Pollack, I. B., Flocke, F., Wolfe, G. M., Hanisco, T. F., Keutsch, F. N., Kaiser, J., Bui, T. P. V., Jimenez, J. L., Campuzano‐Jost, P., Apel, E. C., Hornbrook, R. S., Hills, A. J., Yuan, B., and Wisthaler, A.: Evaluating the Impact of Chemical Complexity and Horizontal Resolution on Tropospheric Ozone Over the Conterminous US With a Global Variable Resolution Chemistry Model, J Adv Model Earth Syst, 14, e2021MS002889, https://doi.org/10.1029/2021MS002889, 2022.

Shen, S., Li, C., van Donkelaar, A., Jacobs, N., Wang, C., and Martin, R. V.: Enhancing Global Estimation of Fine Particulate Matter Concentrations by Including Geophysical a Priori Information in Deep Learning, ACS EST Air, 1, 332–345, https://doi.org/10.1021/acsestair.3c00054, 2024.

Sun, R., Lu, X., Gao, M., Du, Y., Lin, H., Wright, C., He, C., and Yin, K.: The impacts of shipping emissions on lightning: roles of aerosol-radiation-interactions and aerosol-cloud-interactions, Environ. Res. Lett., 19, 034038, https://doi.org/10.1088/1748-9326/ad2aba, 2024.

Sun, R. (2025). model output for BCC-GEOS-Chem v2.0. Zenodo. https://doi.org/10.5281/zenodo.16734757

Sun, R. (2026a). BCC-GEOS-Chem v2.0 code. Zenodo. https://doi.org/10.5281/zenodo.18448688

Sun, R. (2026b). HEMCO module in BCC-GEOS-Chem v2.0. Zenodo. https://doi.org/10.5281/zenodo.18862941

Tarasick, D., Galbally, I. E., Cooper, O. R., Schultz, M. G., Ancellet, G., Leblanc, T., Wallington, T. J., Ziemke, J., Liu, X., Steinbacher, M., Staehelin, J., Vigouroux, C., Hannigan, J. W., García, O., Foret, G., Zanis, P., Weatherhead, E., Petropavlovskikh, I., Worden, H., Osman, M., Liu, J., Chang, K.-L., Gaudel, A., Lin, M., Granados-Muñoz, M., Thompson, A. M., Oltmans, S. J., Cuesta, J., Dufour, G., Thouret, V., Hassler, B., Trickl, T., and Neu, J. L.: Tropospheric Ozone Assessment Report: Tropospheric ozone from 1877 to 2016, observed levels, trends and uncertainties, Elementa: Science of the Anthropocene, 7, 39, https://doi.org/10.1525/elementa.376, 2019.

Twomey, S.: The Influence of Pollution on the Shortwave Albedo of Clouds, Journal of the Atmospheric Sciences, 34, 1149–1152, https://doi.org/10.1175/1520-0469(1977)034<1149:TIOPOT>2.0.CO;2, 1977.

Wang, C., Soden, B. J., Yang, W., and Vecchi, G. A.: Compensation Between Cloud Feedback and Aerosol‐Cloud Interaction in CMIP6 Models, Geophysical Research Letters, 48, e2020GL091024, https://doi.org/10.1029/2020GL091024, 2021a.

Wang, H., Lu, X., Jacob, D. J., Cooper, O. R., Chang, K.-L., Li, K., Gao, M., Liu, Y., Sheng, B., Wu, K., Wu, T., Zhang, J., Sauvage, B., Nédélec, P., Blot, R., and Fan, S.: Global tropospheric ozone trends, attributions, and radiative impacts in 1995–2017: an integrated analysis using aircraft (IAGOS) observations, ozonesonde, and multi-decadal chemical model simulations, Atmospheric Chemistry and Physics, 22, 13753–13782, https://doi.org/10.5194/acp-22-13753-2022, 2022.

Wang, H., Lu, X., Palmer, P. I., Zhang, L., Lu, K., Li, K., Nagashima, T., Koo, J.-H., Tanimoto, H., Wang, H., Gao, M., He, C., Wu, K., Fan, S., and Zhang, Y.: Deciphering decadal urban ozone trends from historical records since 1980, National Science Review, 11, nwae369, https://doi.org/10.1093/nsr/nwae369, 2024.

Wang, J., Jacob, D. J., and Martin, S. T.: Sensitivity of sulfate direct climate forcing to the hysteresis of particle phase transitions, J. Geophys. Res., 113, 2007JD009368, https://doi.org/10.1029/2007JD009368, 2008.

Wang, X., Jacob, D. J., Downs, W., Zhai, S., Zhu, L., Shah, V., Holmes, C. D., Sherwen, T., Alexander, B., Evans, M. J., Eastham, S. D., Neuman, J. A., Veres, P. R., Koenig, T. K., Volkamer, R., Huey, L. G., Bannan, T. J., Percival, C. J., Lee, B. H., and Thornton, J. A.: Global tropospheric halogen (Cl, Br, I) chemistry and its impact on oxidants, Atmospheric Chemistry and Physics, 21, 13973–13996, https://doi.org/10.5194/acp-21-13973-2021, 2021b.

Weng, H., Lin, J., Martin, R., Millet, D. B., Jaeglé, L., Ridley, D., Keller, C., Li, C., Du, M., and Meng, J.: Global high-resolution emissions of soil NOx, sea salt aerosols, and biogenic volatile organic compounds, Sci Data, 7, 148, https://doi.org/10.1038/s41597-020-0488-5, 2020.

Wesely, M. L.: Parameterization of surface resistances to gaseous dry deposition in regional-scale numerical models, Atmospheric Environment (1967), 23, 1293–1304, https://doi.org/10.1016/0004-6981(89)90153-4, 1989.

Wild, O. and Prather, M. J.: Global tropospheric ozone modeling: Quantifying errors due to grid resolution, Journal of Geophysical Research: Atmospheres, 111, https://doi.org/10.1029/2005JD006605, 2006.

Wu, T., Lu, Y., Fang, Y., Xin, X., Li, L., Li, W., Jie, W., Zhang, J., Liu, Y., Zhang, L., Zhang, F., Zhang, Y., Wu, F., Li, J., Chu, M., Wang, Z., Shi, X., Liu, X., Wei, M., Huang, A., Zhang, Y., and Liu, X.: The Beijing Climate Center Climate System Model (BCC-CSM): the main progress from CMIP5 to CMIP6, Geosci. Model Dev., 12, 1573–1600, https://doi.org/10.5194/gmd-12-1573-2019, 2019.

Wu, T., Zhang, F., Zhang, J., Jie, W., Zhang, Y., Wu, F., Li, L., Yan, J., Liu, X., Lu, X., Tan, H., Zhang, L., Wang, J., and Hu, A.: Beijing Climate Center Earth System Model version 1 (BCC-ESM1): model description and evaluation of aerosol simulations, Geosci. Model Dev., 13, 977–1005, https://doi.org/10.5194/gmd-13-977-2020, 2020.

Wu, T., Li, W., Ji, J., Xin, X., Li, L., Wang, Z., Zhang, Y., Li, J., Zhang, F., Wei, M., Shi, X., Wu, F., Zhang, L., Chu, M., Jie, W., Liu, Y., Wang, F., Liu, X., Li, Q., Dong, M., Liang, X., Gao, Y., and Zhang, J.: Global carbon budgets simulated by the Beijing Climate Center Climate System Model for the last century, n.d.

Young, P. J., Naik, V., Fiore, A. M., Gaudel, A., Guo, J., Lin, M. Y., Neu, J. L., Parrish, D. D., Rieder, H. E., Schnell, J. L., Tilmes, S., Wild, O., Zhang, L., Ziemke, J., Brandt, J., Delcloo, A., Doherty, R. M., Geels, C., Hegglin, M. I., Hu, L., Im, U., Kumar, R., Luhar, A., Murray, L., Plummer, D., Rodriguez, J., Saiz-Lopez, A., Schultz, M. G., Woodhouse, M. T., and Zeng, G.: Tropospheric Ozone Assessment Report: Assessment of global-scale model performance for global and regional ozone distributions, variability, and trends, Elementa: Science of the Anthropocene, 6, 10, https://doi.org/10.1525/elementa.265, 2018.

Yu, F. and Luo, G.: Simulation of particle size distribution with a global aerosol model: contribution of nucleation to aerosol and CCN number concentrations, Atmospheric Chemistry and Physics, 9, 7691–7710, https://doi.org/10.5194/acp-9-7691-2009, 2009.

Yu, K., Jacob, D. J., Fisher, J. A., Kim, P. S., Marais, E. A., Miller, C. C., Travis, K. R., Zhu, L., Yantosca, R. M., Sulprizio, M. P., Cohen, R. C., Dibb, J. E., Fried, A., Mikoviny, T., Ryerson, T. B., Wennberg, P. O., and Wisthaler, A.: Sensitivity to grid resolution in the ability of a chemical transport model to simulate observed oxidant chemistry under high-isoprene conditions, Atmos. Chem. Phys., 16, 4369–4378, https://doi.org/10.5194/acp-16-4369-2016, 2016.

Zelinka, M. D., Andrews, T., Forster, P. M., and Taylor, K. E.: Quantifying components of aerosol-cloud-radiation interactions in climate models, J. Geophys. Res. Atmos., 119, 7599–7615, https://doi.org/10.1002/2014JD021710, 2014.

Zender, C. S., Bian, H., and Newman, D.: Mineral Dust Entrainment and Deposition (DEAD) model: Description and 1990s dust climatology, Journal of Geophysical Research: Atmospheres, 108, https://doi.org/10.1029/2002JD002775, 2003.

Zhang, L.: A size-segregated particle dry deposition scheme for an atmospheric aerosol module, Atmospheric Environment, 35, 549–560, https://doi.org/10.1016/S1352-2310(00)00326-5, 2001.

Zhang, L., Jacob, D. J., Liu, X., Logan, J. A., Chance, K., Eldering, A., and Bojkov, B. R.: Intercomparison methods for satellite measurements of atmospheric composition: application to tropospheric ozone from TES and OMI, Atmospheric Chemistry and Physics, 10, 4725–4739, https://doi.org/10.5194/acp-10-4725-2010, 2010.

Zhang, X., Zhang, Q., Hong, C., Zheng, Y., Geng, G., Tong, D., Zhang, Y., and Zhang, X.: Enhancement of PM 2.5 Concentrations by Aerosol - Meteorology Interactions Over China, JGR Atmospheres, 123, 1179–1194, https://doi.org/10.1002/2017JD027524, 2018.

Zhao, B., Liou, K.-N., Gu, Y., Li, Q., Jiang, J. H., Su, H., He, C., Tseng, H.-L. R., Wang, S., Liu, R., Qi, L., Lee, W.-L., and Hao, J.: Enhanced PM2.5 pollution in China due to aerosol-cloud interactions, Sci Rep, 7, 4453, https://doi.org/10.1038/s41598-017-04096-8, 2017.

Zhao, M., Dai, T., Wang, H., Bao, Q., Liu, Y., Zhang, H., and Shi, G.: Sensitivities of simulated global aerosol optical depth and aerosol-radiation interactions to different horizontal resolutions in CAS-FGOALS-f3, Atmospheric Environment, 271, 118920, https://doi.org/10.1016/j.atmosenv.2021.118920, 2022.

Zhao, Y., Saunois, M., Bousquet, P., Lin, X., Hegglin, M. I., Canadell, J. G., Jackson, R. B., and Zheng, B.: Reconciling the bottom-up and top-down estimates of the methane chemical sink using multiple observations, Atmos. Chem. Phys., 23, 789–807, https://doi.org/10.5194/acp-23-789-2023, 2023.

Zhou, M., Zhang, L., Chen, D., Gu, Y., Fu, T.-M., Gao, M., Zhao, Y., Lu, X., and Zhao, B.: The impact of aerosol–radiation interactions on the effectiveness of emission control measures, Environ. Res. Lett., 14, 024002, https://doi.org/10.1088/1748-9326/aaf27d, 2019.

Zhu, L., Jacob, D. J., Kim, P. S., Fisher, J. A., Yu, K., Travis, K. R., Mickley, L. J., Yantosca, R. M., Sulprizio, M. P., De Smedt, I., González Abad, G., Chance, K., Li, C., Ferrare, R., Fried, A., Hair, J. W., Hanisco, T. F., Richter, D., Jo Scarino, A., Walega, J., Weibring, P., and Wolfe, G. M.: Observing atmospheric formaldehyde (HCHO) from space: validation and intercomparison of six retrievals from four satellites (OMI, GOME2A, GOME2B,OMPS) with SEAC4 RS aircraft observations over the southeast US, Atmos. Chem. Phys., 16, 13477–13490, https://doi.org/10.5194/acp-16-13477-2016, 2016.

Zhu, L., González Abad, G., Nowlan, C. R., Chan Miller, C., Chance, K., Apel, E. C., DiGangi, J. P., Fried, A., Hanisco, T. F., Hornbrook, R. S., Hu, L., Kaiser, J., Keutsch, F. N., Permar, W., St. Clair, J. M., and Wolfe, G. M.: Validation of satellite formaldehyde (HCHO) retrievals using observations from 12 aircraft campaigns, Atmospheric Chemistry and Physics, 20, 12329–12345, https://doi.org/10.5194/acp-20-12329-2020, 2020.

Zhuang, J., Jacob, D. J., and Eastham, S. D.: The importance of vertical resolution in the free troposphere for modeling intercontinental plumes, Atmospheric Chemistry and Physics, 18, 6039–6055, https://doi.org/10.5194/acp-18-6039-2018, 2018.